Photoelectron spectroscopy, gas phase acidity, and thermochemistry of *tert*-butyl hydroperoxide: Mechanisms for the rearrangement of peroxyl radicals

Eileen P. Clifford
Department of Chemistry and Biochemistry, University of Colorado, Boulder, Colorado 80309-0215

Paul G. Wenthold
JILA and the Department of Chemistry and Biochemistry, University of Colorado, Boulder, Colorado 80309-0440

Roustam Gareyev
Department of Chemistry and Biochemistry, University of Colorado, Boulder, Colorado 80309-0215

W. Carl Lineberger
JILA and the Department of Chemistry and Biochemistry, University of Colorado, Boulder, Colorado 80309-0440

Charles H. DePuy, Veronica M. Bierbaum, and G. Barney Ellison
Department of Chemistry and Biochemistry, University of Colorado, Boulder, Colorado 80309-0215

(Received 16 December 1997; accepted 26 March 1998)

The 3.531 eV negative ion photoelectron spectra of the hydroperoxide ion and the *tert*-butylperoxide ion have been studied. We find $HO_2^- + \hbar\omega_{351.1\,nm} \rightarrow HO_2 + e^-$ $EA[HO_2, \tilde{X}\ ^2A'']$ $= 1.089 \pm 0.006$ eV, $(CH_3)_3COO^- + \hbar\omega_{351.1\,nm} \rightarrow (CH_3)_3COO + e^-$ $EA[(CH_3)_3COO, \tilde{X}\ ^2A''] = 1.196$ ± 0.011 eV. The photoelectron spectra show detachment to the ground state of the peroxyl radicals and to a low lying electronic state. The intercombination gaps are measured to be $\Delta E(\tilde{X}\ ^2A'' - \tilde{A}\ ^2A')[HO_2] = 0.871 \pm 0.007$ eV and $\Delta E(\tilde{X}\ ^2A'' - {}^2A')[(CH_3)_3COO] = 0.967 \pm 0.011$ eV. The gas phase acidity of $(CH_3)_3COOH$ was measured in a tandem flowing afterglow-selected ion flow tube (FA-SIFT) to be $\Delta_{acid}G_{298} = 363.2 \pm 2.0$ kcal mol^{-1} and we find $\Delta_{acid}H_{298}[(CH_3)_3COO{-}H] = 370.9 \pm 2.0$ kcal mol^{-1}. Use of $\Delta_{acid}H_{298}[(CH_3)_3COO{-}H]$ and $EA[(CH_3)_3COO]$ leads to the bond energies $DH_{298}[(CH_3)_3COO{-}H] = 85 \pm 2$ kcal mol^{-1} and $D_0[(CH_3)_3COO{-}H] = 83 \pm 2$ kcal mol^{-1}. The thermochemistry of the alkylperoxyl radicals, RO_2, is reviewed. A mechanism for the rearrangement of chemically activated peroxyl radicals is proposed $[RO_2]\tilde{X}\ ^2A'' \rightarrow [RO_2]^*\tilde{A}\ ^2A' \rightarrow$ aldehydes/ketones $+ HO(^2\Pi)$, $[RO_2]\tilde{X}\ ^2A'' \rightarrow [RO_2]^*\tilde{A}\ ^2A' \rightarrow$ alkenes $+ HO_2(\tilde{X}\ ^2A'')$. © *1998 American Institute of Physics.* [S0021-9606(98)01925-4]

I. INTRODUCTION

Atmospheric oxidation of hydrocarbons leads to the formation of peroxyl radicals, which have a rich literature.[1–4] Radical abstraction of a hydrogen atom from hydrocarbons (RH) generates the resulting alkyl radical, R, which readily adds O_2 to form peroxyl radicals (RO_2). In the troposphere, peroxyl radicals are a crucial link[5,6] in the formation of tropospheric ozone

$$R + O_2 + M \rightarrow RO_2 + M, \tag{1}$$

$$RO_2 + NO \rightarrow [ROONO] \rightarrow RO + NO_2, \tag{2}$$

$$NO_2 + \text{sunlight} \rightarrow NO + O(^3P), \tag{3}$$

$$O(^3P) + O_2 + M \rightarrow O_3 + M. \tag{4}$$

Reactions (1) and (2) are fast,[7,8] $k_1 = 8 \times 10^{-11}$ cm^3 molecule^{-1} s^{-1} and $k_2 \cong 8{-}11 \times 10^{-12}$ cm^3 molecule^{-1} s^{-1}.

In combustion processes, alkylperoxyl radicals are formed by the rapid addition of alkyl radicals to oxygen. The HRO_2 radicals produce different products at varying temperatures, and the rearrangement product RO_2H is of practical interest since it is implicated in ''engine knock,'' which limits the temperature range (and efficiency) of internal combustion engines,[9]

$$C_NH_MCH_2{-}CH_2OO \rightarrow [C_NH_MCH{-}CH_2OOH] \rightarrow C_NH_MCH{=}CH_2 + HO_2. \tag{5}$$

There is a spectacular prediction[10,11] about the formation and reactivity of the vinylperoxyl, $CH_2{=}CH{-}O_2$, and phenylperoxyl, $C_6H_5{-}O_2$, radicals. These species are key inter-

TABLE I. Experimental constants for the hydroperoxyl radical (HO_2).

			Ref.
$\tilde{X}\ ^2A''$ state			
$\nu_1 = 3436.20\ cm^{-1}$	OH stretch	$r_e = 0.9754 \pm 0.0021$ Å	32, 34, 35
$\nu_2 = 1391.75\ cm^{-1}$	Bend	$\theta_e = 104.02 \pm 0.24°$	
$\nu_3 = 1097.63\ cm^{-1}$	OO stretch	$r_e = 1.3291 \pm 0.0006$ Å	
$A_0 = 20.356\ cm^{-1}$, $B_0 = 1.118\ cm^{-1}$, $C_0 = 1.056\ cm^{-1}$			35
$\tilde{A}\ ^2A' \leftarrow \tilde{X}\ ^2A''$ 7029.684±0.002 cm^{-1} (0.871 574 5±0.000 000 2 eV)			33, 34, 57
$\tilde{A}\ ^2A'$ state			
$\nu_1 = 3268.5\ cm^{-1}$	OH stretch	$r_e = 0.9654 \pm 0.0011$ Å	
$\nu_2 = 1285\ cm^{-1}$	Bend	$\theta_e = 102.69 \pm 0.12°$	
$\nu_3 = 929.068\ cm^{-1}$	OO stretch	$r_e = 1.3933 \pm 0.0003$ Å	
$A_0 = 20.486\ cm^{-1}$, $B_0 = 1.021\ cm^{-1}$, $C_0 = 0.968\ cm^{-1}$			35
$\tilde{B}\ ^2A''$ dissociative state absorbs 200–280 nm, peaks at 205 nm (4.4–6.2 eV)			14
	D_0 /kcal mol^{-1}	DH_{298} /kcal mol^{-1}	15
D(HOO–H)	86±1	88±1	
D(HO–OH)	49.7±0.1	51.3±0.1	
D(H–O_2)	48±1	49±1	
D(HO–O)	65±1	66±1	
$AP(HO_2^+, H_2O_2) = 15.115 \pm 0.035$ eV			15
$IP(HO_2) = 11.352 \pm 0.007$ eV			
$\Delta_f H_0(HO_2^+) = 257.7 \pm 0.8$ kcal mol^{-1}			
$EA(HO_2) = 1.078 \pm 0.017$ eV			20, 21
Principal values of the g-tensor from the EPR spectrum of matrix isolated HO_2: $g_1 = 2.0344$, $g_2 = 2.0087$, $g_3 = 2.0031$			75

mediates in the oxidative destruction of hydrocarbons (in particular aromatic molecules) and studies of these species are just beginning.[12,13] The predicted cyclization and fragmentation of these unsaturated peroxyl radicals are important reactions and, if proven, demonstrate the remarkable versatility of these species.

In order to understand the chemistry of alkyl peroxyl radicals, it is essential to have an accurate grasp of the thermochemistry, spectroscopy, and dynamics of these species. We restrict the subject of this paper to the saturated alkyl peroxyl radicals; the properties of CH_2CHO_2 and $C_6H_5O_2$ will be investigated in future studies. An exhaustive review of peroxyl radicals has recently appeared.[14]

The simplest peroxyl radical is hydroperoxyl, HO_2, and it has been well studied in the laboratory as well as in the atmosphere.[15] The structure of the hydroperoxyl radical is dictated[16,17] by that of O_2 and we can represent[18] the low-lying states of HO_2 as in (6).

HO_2^-	HO_2	HO_2	HO_2
$\tilde{X}\ ^1A'$	$\tilde{X}\ ^2A''$	$\tilde{A}\ ^2A'$	$\tilde{B}\ ^2A''$
-1.089 ± 0.006 eV	0.0	0.871 574 5±0.000 000 2 eV	4.4–6.2 eV.

(6)

Some of the values for bond lengths and energy splittings have been previously studied and are listed in Table I.

This paper reports our investigations of the spectroscopic and thermochemical properties for the simple alkylperoxyl radical, *tert*-butyl peroxyl. Table II lists the previously reported parameters for $(CH_3)_3COO$. By combining the experiments of (a) negative ion photoelectron spectroscopy, and (b) gas phase acidity measurements,[19] we are able to measure the electron affinity (EA) of the peroxyl radical, the splitting between electronic states, the peroxyl radical's vibrations excited by photodetachment, and the enthalpy of deprotonation ($\Delta_{acid}H_{298}$) of the parent *tert*-butylhydroperoxide. These parameters for $(CH_3)_3COO$ will be compared to those for HO_2. We expect the photodetachment spectra for HO_2^- (which has been examined earlier)[20,21] and that of $(CH_3)_3COO^-$ to be quite similar.

Expression (7) shows the GVB representations[17] of the $\tilde{X}\ ^1A'$ *tert*-butyl peroxyl anion and the $\tilde{X}\ ^2A''$, $\tilde{A}\ ^2A'$, and $\tilde{B}\ ^2A''$ states of the *tert*-butyl peroxyl radicals with estimates for state separations based on those of HO_2,

TABLE II. Experimental parameters of $(CH_3)_3COO$ $\tilde{X}\ ^2A''/cm^{-1}$. (a) Vibrational spectrum. (b) Thermodynamics.

	$(CH_3)_3CO_2$/gas	$(CH_3)_3C^{16}O_2$/Ar matrix	$(CH_3)_3C^{18}O_2$/Ar	Ref.
(a)				
CH_3 rock		1187±2	1184±2	36
CH_3 rock		1139±2	1141±2	36
OO stretch		1124±2	1070±2	36
CC stretch		808±2	805±2	36
	760 ±2			76
CO stretch		730±2	707±2	36
	693.7±0.5			76
Skeletal bends		539±2	529±2	36
		403±2	400±2	36
		361±2	356±2	36
		337±2	333±2	36
(b)				
$DH_{298}[(CH_3)_3C-O_2]=36.7\pm1.9$ kcal mol^{-1}				45
$\Delta_f H_{298}[(CH_3)_3C]=11.6\pm0.4$ kcal mol^{-1}				41, 77
$\Delta_f H_{298}[(CH_3)_3COO]=-25.1\pm1.9$ kcal mol^{-1}				45
Principal values of the g-tensor from the EPR spectrum of $(CH_3)_3COO$ in a D_2O matrix; $g_1=2.0288$, $g_2=2.0085$, $g_3=2.0029$				78

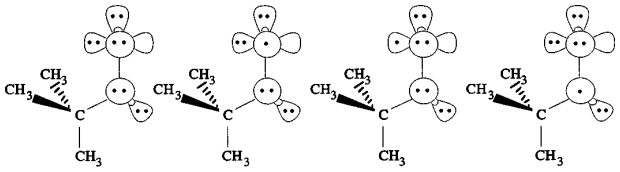

$$\begin{array}{cccc} (CH_3)_3COO^- & (CH_3)_3COO & (CH_3)_3COO & (CH_3)_3COO \\ \tilde{X}\ ^1A' & \tilde{X}\ ^2A'' & \tilde{A}\ ^2A' & \tilde{B}\ ^2A'' \\ \Delta E\cong -1\ \text{eV} & 0.0 & \Delta E\cong 1\ \text{eV} & \Delta E\cong 5\ \text{eV}. \end{array} \tag{7}$$

Equation (8) summarizes the negative ion photodetachment experiment. The vibrations most likely to be excited in the radical $(CH_3)_3COO$ are modes dictated by geometry changes from the anion to the radical,

$$\tilde{X}\ ^1A'(CH_3)_3COO^- + \hbar\omega_0 \rightarrow (CH_3)_3COO\ \tilde{X}\ ^2A'' + e^-. \tag{8}$$

Expression (7) suggests that upon photodetachment, the radical is anticipated to have an excited O–O stretch due to differences in the O–O bond length between the anion and the neutral. The vibration corresponding to bending of the O–O–X [X=H,$(CH_3)_3C$] angle may also be excited, although less of a geometry change is expected for the bond angle. The $(CH_3)_3C$ group is expected to stabilize the extra electron in the anion better than does the H atom, so the electron affinity of $(CH_3)_3COO$ is expected to be higher than that of HO_2.

II. EXPERIMENT

A. Negative ion photoelectron detachment

The negative ions were created in a flowing afterglow apparatus that has been previously described.[22] *Tert*-butyl hydroperoxide was purchased from Aldrich; approximately 90% pure H_2O_2 was prepared from standard 30% H_2O_2 from Aldrich by bubbling N_2 through the mixture to evaporate the water. These two precursors were used without further purification. Vapor from the precursor was introduced into the flowing afterglow by means of a leak valve, with the largest ion beams obtained when the peroxides had minimal contact with metal tubing. The precursor was deprotonated by O^- created from O_2 which was added before the microwave discharge. The negative ions HO_2^- and $(CH_3)_3COO^-$ were selected by a Wien velocity filter before being photodetached by light from a circulating build-up cavity fed by a fixed frequency argon ion laser at 351.1 nm (3.531 eV). Photodetached electrons were focused and passed through a hemispherical energy analyzer. In order to reduce rotational broadening in the photodetachment spectra, the flow tube is cooled with liquid N_2, producing ion temperatures of 200 K±30 K.

The photoelectron spectra are calibrated[23] with respect to O^- and transformed to the center of mass (cm) frame by a standard[24] expression where E is the cm kinetic energy (eV) of an electron detached from an ion of mass M (amu) which is passed by the energy analyzer when the slit voltage is V. The beam energy is W, m_e is the mass of an electron, and γ is the dimensionless scale compression factor (typically 1.000±0.006),

$$E = E_{\text{cal}} + \gamma(V - V_{\text{cal}}) + m_e W\left(\frac{1}{M_{\text{cal}}} - \frac{1}{M}\right). \tag{9}$$

B. Flowing afterglow selected ion flow tube measurements

The gas phase acidity of *tert*-butyl hydroperoxide $[\Delta_{\text{acid}}G_{298}((CH_3)_3COOH)]$ was measured using a tandem flowing afterglow-selected ion flow tube (FA-SIFT) apparatus.[25] Two independent methods were employed to establish the acidity of this compound. The first approach[26] involved the measurement of the rate constant for proton

transfer between *tert*-butyl hydroperoxide (HA) and a conjugate base (B^-) of a reference acid, as well as the rate constant for the reverse reaction,

$$HA + B^- \rightleftharpoons A^- + HB. \tag{10}$$

The ratio of the two rate constants k_{10} and k_{-10} gives the proton transfer equilibrium constant $K_{equi}(10)$, which is related in a simple way to the difference in gas phase acidities of the two compounds,

$$\Delta_{acid}G_T(HA) - \Delta_{acid}G_T(HB) = \Delta\Delta G_{acid} = -RT \ln K_{equi}(10). \tag{11}$$

The second method[27] is that of Cooks and co-workers; the approach is based on collision-induced dissociation (CID) of ion–molecule complexes $[A\cdots H\cdots B]^-$, which yields fragment ions A^- and B^- in a ratio which reflects their relative basicity,

$$[A\cdots H\cdots B]^- \xrightarrow{k_{12a}} A^- + HB \qquad [A\cdots H\cdots B]^- \xrightarrow{k_{12b}} HA + B^- \tag{12}$$

$$\Delta\Delta G_{acid} = -\alpha RT \ln\left[\frac{k_{12a}}{k_{12b}}\right] = -\alpha RT \ln\left[\frac{(A^-)}{(B^-)}\right]. \tag{13}$$

The method is most reliable when the components of the cluster are chemically and structurally similar, so that entropy differences between the two dissociation channels are minimized.[27–29] The calibration coefficient α in Eq. (13) may be unity or greater depending on specific experimental conditions. It may be determined from calibration plots of $\ln([A^-]/[B^-])$ vs known $\Delta\Delta G_{acid}$ values for compounds of similar structure.[28,29]

The hydrogen bonded clusters used in the second (kinetic) method, $[(CH_3)_3COO^-\cdot HOR]$ and $[R_1O^-\cdot HOR_2]$, were generated by chemical ionization of a mixture of the two parent compounds by the OH^- precursor in a flow of helium buffer gas (0.2 Torr). Precursor ions were generated upstream in the flow tube by electron impact on the mixture of N_2O and CH_4. The dissociative ionization of N_2O yields O^- which rapidly abstracts a hydrogen atom from methane to give OH^-. The cluster of interest was mass selected in the SIFT quadrupole and injected into the second flow tube (0.5 Torr of helium) at a laboratory frame kinetic energy of approximately 25 eV. The observed abundances of the two fragment anions were corrected to account for mass discrimination of the detection system. The correction factor for the difference in sensitivity at the extremes of mass detection [mass-to-charge ratios 87 and 107 for $(CH_3)_3CCH_2O^-$ and $C_6H_5CH_2O^-$, respectively] was typically 1.2 and did not exceed 1.5.

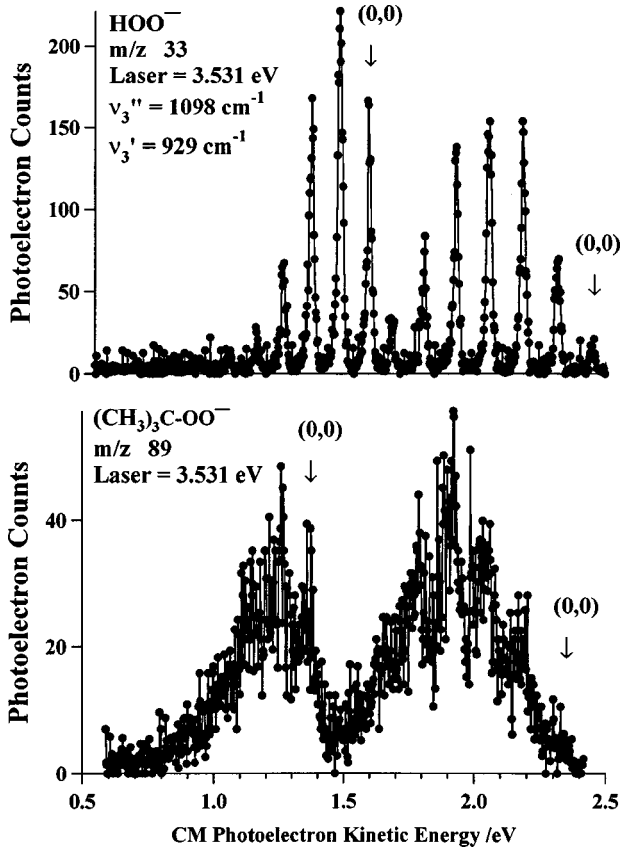

FIG. 1. A comparison of the negative ion photoelectron spectrum of the HO_2^- and $(CH_3)_3COO^-$ ions. For HO_2^- the (0,0) features occur at electron kinetic energies of 2.447 ± 0.002 eV and 1.575 ± 0.003 eV while $(CH_3)_3COO^-$ has transitions at 2.335 ± 0.005 eV and 1.368 ± 0.005 eV.

III. EXPERIMENTAL RESULTS

A. Negative ion photoelectron detachment

Figure 1 illustrates the similarities between the photodetachment spectra of the two peroxide anions, HO_2^- and $(CH_3)_3COO^-$. In each spectrum, two major progressions mark the two electronic states, ROO $\tilde{X}\ ^2A''$ and ROO $\tilde{A}\ ^2A'$. In the HO_2^- spectrum, each electronic state has one vibrational mode excited; in the $(CH_3)_3COO^-$ spectrum, both states appear to have two active modes. The electron affinities and separations between electronic states are similar for the two peroxyl radicals.

The HO_2^- fitted spectrum is displayed in Fig. 2. The present data for HO_2 agrees well with previous experiments. Table III lists the raw peak positions obtained for the photodetachment spectra of HO_2^- and $(CH_3)_3COO^-$. The ''raw'' electron affinity of HO_2^- was extracted from the (0,0) band at 2.447 eV and yields a value of 1.084 eV. We use an approximate rotational correction (using calculated and known rotational constants) to identify the final electron affinity.[30] In the $\tilde{X}\ ^2A''$ state, the (0,0) transition is 0.005 eV from the center of the peak due to the rotational profile underneath, and in the $\tilde{A}\ ^2A'$ state, an adjustment of 0.004 eV must be made. We have used calculated rotational constants to estimate the peak broadening in the spectra due to rotational transitions.[31] We find that the calculated peak width for HO_2 is 24 meV, close to the observed value of 29 meV. To calculate the

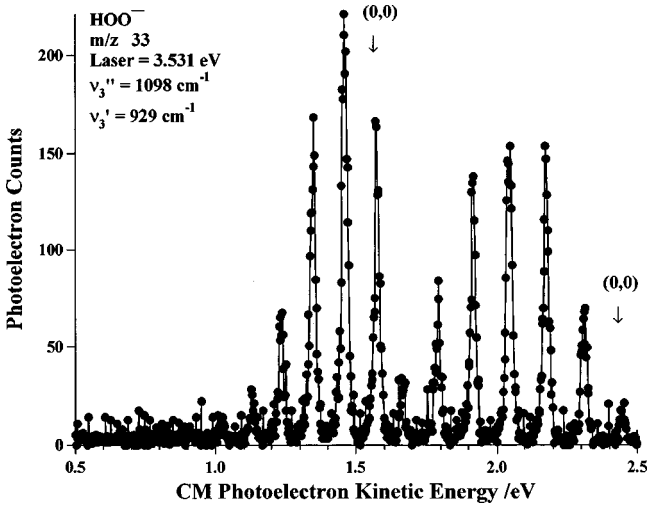

FIG. 2. A plot of the fitted spectrum of the $\tilde{X}\ ^2A''$ and the $\tilde{A}\ ^2A'$ states of HOO.

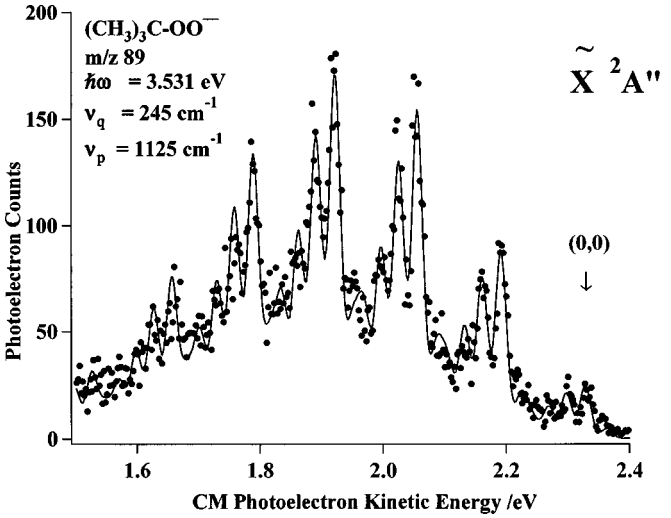

FIG. 3. An expanded plot of the vibronic fine structure of the $\tilde{X}\ ^2A''$ state of $(CH_3)_3COO$. The active modes are $\nu_p = 1130 \pm 90\ cm^{-1}$ and $\nu_q = 245 \pm 90\ cm^{-1}$.

TABLE III. Negative ion photoelectron uncorrected peak positions. CM kinetic energy/eV for the most prominent transitions/eV. Ar III laser $\lambda_0 = 351.1$ nm (3.531 eV).

(I) $HO_2^- + \hbar\omega_0 \rightarrow HO_2 + e^-$(KE)		
The active mode is ν_3, the HO–O stretch		
$\tilde{X}\ ^2A''$	(0,0)	2.447 eV
	3_0^1	2.311
	3_0^2	2.177
	3_0^3	2.046
	3_0^4	1.917
	3_0^5	1.790
	3_0^6	1.664
$\tilde{A}\ ^2A'$	(0,0)	1.575
	3_0^1	1.460
	3_0^2	1.349
	3_0^3	1.237
	3_0^4	1.131
	3_0^5	1.023
(II) $(CH_3)_3COO^- + \hbar\omega_0 \rightarrow (CH_3)_3COO + e^-$(KE)		
The active modes are labeled ν_p, ν_q, ν_r, and ν_s		
$\tilde{X}\ ^2A''$	(0,0)	2.335 eV
	q_0^1	2.305
	p_0^1	2.194
	$q_0^1 p_0^1$	2.163
	p_0^2	2.054
	$q_0^1 p_0^2$	2.023
	p_0^3	1.919
$\tilde{A}\ ^2A'$	(0,0)	1.368
	s_0^1	1.339
	s_0^2	1.309
	r_0^1	1.253
	$s_0^1 r_0^1$	1.222
	$s_0^2 r_0^1$	1.192
	r_0^2	1.138
	$s_0^1 r_0^2$	1.106
	$s_0^2 r_0^2$	1.077

uncertainty in the values, one must take into account the reproducibility of the measurements (0.004 eV), the instrumental uncertainty (0.006 eV), and an estimate for the rotational correction (0.001 eV).

Use of these corrections gives the final value for $EA(HO_2) = 1.089 \pm 0.006$ eV, in good agreement with the value of 1.078 ± 0.017 eV reported previously.[21] The hydroperoxyl spectrum was fit with the established O–O stretch vibrational frequencies of $\nu_3 = 1097.63\ cm^{-1}$ for the $\tilde{X}$ state and $\nu_3 = 929.068\ cm^{-1}$ for the $\tilde{A}$ state.[32] The splitting $\Delta E(\tilde{A}\ ^2A' \leftarrow \tilde{X}\ ^2A'') = 0.871 \pm 0.007$ eV from our photoelectron spectrum is in excellent agreement with the previously measured splitting of $7029.684 \pm 0.002\ cm^{-1}$(0.871 574 5 $\pm$0.000 000 2 eV).[32–35]

The spectrum of $(CH_3)_3COO^-$ is analyzed by analogy to that of HO_2^- as the overview spectrum in Fig. 1 implies. Figure 3 is an expanded view of the photoelectron spectrum of the $\tilde{X}\ ^2A''$ state of $(CH_3)_3COO$, with our fit. Detachment to $(CH_3)_3COO\ \tilde{X}\ ^2A''$ excites at least two vibrations that will be labeled ν_p and ν_q. The electron affinity of $(CH_3)_3COO$ is labeled as (0,0) and is assigned 1.196 ± 0.011 eV, greater than that of HO_2. Use of calculated rotational constants indicates that the rotational origin is not shifted from the center of the peak, so no corrections are made. The uncertainty will be discussed below. The empirical fit to the spectrum found a frequency of $\nu_p = 1130 \pm 90\ cm^{-1}$ comparable to the O–O stretch frequency of $1098\ cm^{-1}$ observed in HO_2. A frequency of $1124 \pm 10\ cm^{-1}$ has been assigned to the O–O stretch of $(CH_3)_3COO$ in an argon matrix.[36] The other active mode was found to be $\nu_q = 245 \pm 90\ cm^{-1}$.

Figure 4 shows the fit to the $\tilde{A}\ ^2A'$ state of $(CH_3)_3COO$ and the two active modes are labeled ν_r and ν_s. In the excited state, $\nu_r = 930 \pm 90\ cm^{-1}$ and $\nu_s = 240 \pm 90\ cm^{-1}$ (similar to the $929\ cm^{-1}$ O–O stretch in $\tilde{A}\ ^2A'\ HO_2$) were used to fit the spectrum. The *tert*-butyl peroxyl intercombination gap indicated as (0,0) was found to be greater than that of HO_2, and is $\Delta E[(CH_3)_3COO, \tilde{A}\ ^2A' \leftarrow \tilde{X}\ ^2A''] = 0.967 \pm 0.011$ eV. Pioneering studies[37] of the near IR emissions in alkylperoxyl

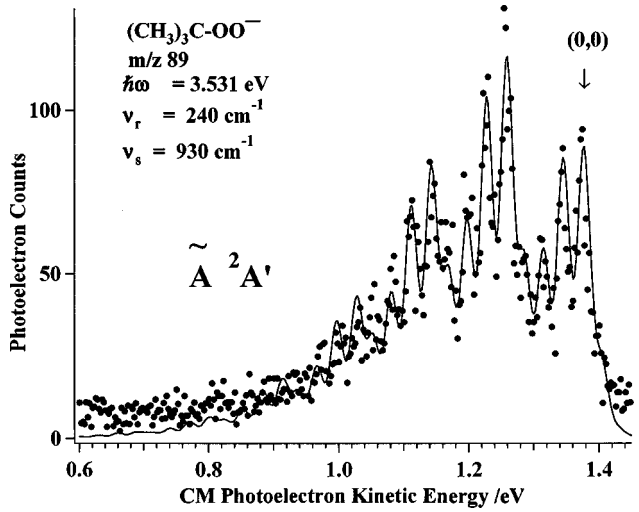

FIG. 4. An expanded plot of the vibronic fine structure of the $\tilde{A}\ ^2A'$ state of $(CH_3)_3COO$. The active modes are $\nu_r = 930 \pm 90\ cm^{-1}$ and $\nu_s = 240 \pm 90\ cm^{-1}$.

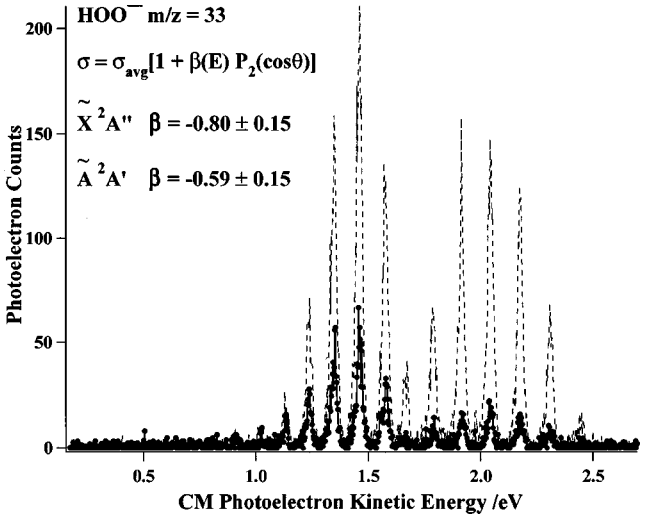

FIG. 5. The angular distribution of photoelectrons from HO_2^-.

radicals led to the discovery of a low lying $^2A'$ state for HO_2, CH_3O_2, and $CH_3CH_2O_2$. The electronic splitting RO_2 $\tilde{A}\ ^2A' \leftarrow \tilde{X}\ ^2A''$ appears to increase with the alkyl group size, CH_3O_2, $T_e = 7375 \pm 2\ cm^{-1}$ (0.9144 ± 0.0002 eV, 1.3559 μm), and for $CH_3CH_2O_2$, $T_e = 7593 \pm 2\ cm^{-1}$ (0.9414 ± 0.0002 eV, 1.3170 μm). Our finding of $T_e[(CH_3)_3CO_2] = 0.967 \pm 0.011$ eV (1.282 μm) follows this trend.

For the $(CH_3)_3COO^-$ spectrum, the peak width for the $\tilde{X}\ ^2A''$ state estimated using calculated rotational constants is 8 meV, and we observe the peak widths in both the $\tilde{X}$ and $\tilde{A}$ states to be approximately 22 meV. Since there is always the possibility that the peaks cannot be described by a simple fit of one frequency to a Gaussian peak, we have adopted error bars for the $(CH_3)_3COO^-$ spectrum accordingly.

The yields of photodetached electrons are angular dependent. The distribution of scattered photoelectrons, $I(\theta)$, is approximated[38,39] by the following expression:

$$I(\theta) = \frac{\overline{\sigma}}{4\pi}\left[1 + \beta(E) P_2(\cos\ \theta)\right]. \tag{14}$$

In this expression, θ is the angle between E_{laser} and the electron collection direction, $\overline{\sigma}$ is the average photodetachment cross section, and $\beta(E)$ is the anisotropy factor which depends on the energy of the scattered electron, E. The anisotropy factor $\beta(E)$ can vary from -1 to $+2$ ($-1 \leqslant \beta \leqslant 2$). The photoelectron spectra shown in Figs. 1–4 are collected under conditions where θ is set to the ''magic angle'' of 54.7° where $P_2(\cos\ \theta) = 0$ so that $I(\theta) = \overline{\sigma}/4\pi$ and is independent of $\beta(E)$. If spectra are collected at $\theta = 0°$ (E_{laser} and collection direction $\parallel$) and $\theta = 90°$ (E_{laser} and collection direction $\perp$), one can extract a value for the anisotropy factor,

$$\beta = \frac{I_{0°} - I_{90°}}{(1/2)\ I_{0°} + I_{90°}}. \tag{15}$$

The value of β provides important information as to the nature of the photodetached electron. In atoms, detachment of an s electron leads to an outgoing p-wave ($l = 1$) and $\beta = +2$, independent of electron kinetic energy. Detachment of a p electron results in a mixture of interfering s- and d-waves and leads to an energy dependent value for $\beta(E)$. At photodetachment threshold, s-wave ($l = 0$) detachment dominates giving $\beta = 0$ and yielding an isotropic photoelectron angular distribution. At photoelectron kinetic energies roughly 1 eV above threshold, d-wave detachment becomes important and $\beta \rightarrow -1$. Electron detachment from molecular ions is more complicated than the atomic case, but β is generally found to be positive for detachment from σ (s-like) electrons and negative for detachment from π (p-like) orbitals.

The asymmetry parameter β measures the change in photodetachment caused by a change in the polarization angle of the laser; it can indicate the character of the orbital of the negative ion from which the electron was detached. For the HO_2^- spectrum in Fig. 5, $\beta = -0.80 \pm 0.15$ for the $\tilde{X}$ state and -0.59 ± 0.15 for the $\tilde{A}$ state. These different values of β indicate detachment from two different orbitals of the negative ion; they are both negative, indicating detachment from π-type orbitals, as predicted from the GVB diagrams. For the $(CH_3)_3COO^-$ spectrum, $\beta = -0.7 \pm 0.2$ for the $\tilde{X}\ ^2A''$ state and $\beta = -0.5 \pm 0.2$ for the $\tilde{A}\ ^2A'$ state. The β values for the two electronic states in both HO_2^- and $(CH_3)_3COO^-$ show similar behavior, with the lower state detaching from a more ''π'' like orbital on the negative ion.

B. *Ab initio* electronic structure calculations

A uniform set of calculations of HO_2^-, HO_2, $(CH_3)_3COO^-$, and $(CH_3)_3COO$ are useful for direct comparison of these species. *Ab initio* electronic structure calculations at the B3LYP/6-311G(d,p) level were performed, using the GAUSSIAN 94 package, for $\tilde{X}\ ^2A''$ HO_2, $\tilde{X}\ ^1A'$ HO_2^-, $\tilde{X}\ ^2A''$ $(CH_3)_3COO$, and $\tilde{X}\ ^1A'$ $(CH_3)_3COO^-$. Table IV compares the change in the peroxyl O–O bond length in the anion and neutral, as well as the X–O–O angle. As Eq. (7) suggests, the change between the negative ion and the peroxyl radical is dramatic; the large difference in the O–O

TABLE IV. *Ab Initio* B3LYP/6-311G(d,p) electronic structure calculations.

(I) Molecular geometries

	$HO_2^-(\tilde{X}\ ^1A')$	$HO_2(\tilde{X}\ ^2A'')$	HO_2 expt[a]	HOOH expt[b]
r_e(O–H)/Å	0.960	0.976	0.9754±0.0021	0.966±0.001
r_e(O–O)/Å	1.532	1.328	1.3291±0.0006	1.467±0.001
∠(HOO)	97.1°	105.5°	104.02±0.24	
τ(HO–OH) torsion				98.84±0.01

	$(CH_3)_3COO^-(\tilde{X}\ ^1A')$	$(CH_3)_3COO(\tilde{X}\ ^2A'')$
$r_e[(CH_3)_3C–OO)]$/Å	1.413	1.503
$r_e[(CH_3)_3CO–O)]$/Å	1.486	1.313
∠$[(CH_3)_3C–O–O)]$	109.1°	113.3°

(II) Harmonic vibrational frequencies (no scaling)

	$HO_2^-\ \tilde{X}\ ^1A'$		$HO_2\ \tilde{X}\ ^2A''$		$HO_2\ \tilde{X}\ ^2A''$
	Freq./cm^{-1}	A/km mol^{-1}	Freq./cm^{-1}	A/km mol^{-1}	Experiment[a]
ω_1	3677	17.9	3533	19.1	ν_1=3436.20
ω_2	1032	16.6	1418	34.9	ν_2=1391.75
ω_3	757	25.1	1162	28.5	ν_3=1097.63

a' modes	$(CH_3)_3COO^-\ \tilde{X}\ ^1A'$ Freq./cm^{-1}	A/km mol^{-1}	a' modes	$(CH_3)_3COO\ \tilde{X}\ ^2A''$ Freq./cm^{-1}	A/km mol^{-1}
ω_1	3075	12.8	ω_1	3127	17.7
ω_2	3058	104.0	ω_2	3112	42.0
ω_3	3043	68.2	ω_3	3105	2.7
ω_4	2997	80.1	ω_4	3044	9.6
ω_5	2981	71.1	ω_5	3037	10.0
ω_6	1518	1.0	ω_6	1523	13.2
ω_7	1490	0.3	ω_7	1499	5.4
ω_8	1474	0.8	ω_8	1489	0.3
ω_9	1377	13.9	ω_9	1425	5.5
ω_{10}	1340	25.2	ω_{10}	1399	24.0
ω_{11}	1263	17.9	ω_{11}	1296	17.9
ω_{12}	1217	44.5	ω_{12}	1219	14.9
ω_{13}	1037	1.7	ω_{13}	1168	20.9
ω_{14}	909	9.1	ω_{14}	1051	0.2
ω_{15}	900	4.3	ω_{15}	933	0.4
ω_{16}	832	7.9	ω_{16}	798	4.2
ω_{17}	735	0.1	ω_{17}	729	3.8
ω_{18}	525	6.4	ω_{18}	543	7.4
ω_{19}	400	0.2	ω_{19}	404	0.7
ω_{20}	369	18.2	ω_{20}	362	3.1
ω_{21}	278	6.3	ω_{21}	272	2.3
ω_{22}	253	2.1	ω_{22}	252	0.1

a'' modes	$(CH_3)_3COO^-\ \tilde{X}\ ^1A'$ Freq./cm^{-1}	A/km mol^{-1}	a'' modes	$(CH_3)_3COO\ \tilde{X}\ ^2A''$ Freq./cm^{-1}	A/km mol^{-1}
ω_1	3070	5.3	ω_1	3123	3.9
ω_2	3065	80.0	ω_2	3112	28.2
ω_3	3036	46.8	ω_3	3104	4.6
ω_4	2971	85.6	ω_4	3038	18.4
ω_5	1496	0.5	ω_5	1498	4.5
ω_6	1470	0.2	ω_6	1491	0.3
ω_7	1448	0.8	ω_7	1470	0.0
ω_8	1322	38.7	ω_8	1398	18.0
ω_9	1229	12.9	ω_9	1262	15.7
ω_{10}	1022	1.3	ω_{10}	1038	0.3
ω_{11}	945	1.7	ω_{11}	969	0.0
ω_{12}	883	4.9	ω_{12}	928	0.0
ω_{13}	471	6.3	ω_{13}	439	3.2
ω_{14}	343	3.4	ω_{14}	332	1.5
ω_{15}	221	0.1	ω_{15}	234	0.0
ω_{16}	197	3.1	ω_{16}	182	0.0
ω_{17}	188	2.6	ω_{17}	131	0.3

[a]Reference 35.
[b]Reference 66.

bond length explains the presence of the progression in the O–O stretch, and the difference in the bond angle hints at the possibility of some bending vibrations.

Table IV lists the B3LYP 6-311G (d,p) *ab initio* harmonic frequencies of these radicals. Since the frequencies of HO_2 are well known, a comparison of the unscaled harmonic frequencies and experimental frequencies is given. The experimental values are lower than the unscaled calculated frequencies. For the $\tilde{X}\ ^2A''$ state of $(CH_3)_3COO$, the a' frequencies corresponding to the fitted values are ω_{21}[$(CH_3)_3C$–O–O bending motion]$=272\ cm^{-1}$ ($\nu_q=245\ cm^{-1}$ experimental) and ω_{13}[$(CH_3)_3CO$–O stretch] $=1168\ cm^{-1}$ ($\nu_p=1130\ cm^{-1}$ experimental). The B3LYP frequencies were also used to estimate $\Delta_{acid}S_{298}$[$(CH_3)_3COOH$] and C_p[$(CH_3)_3COOH$], which are required to find $\Delta_{acid}H_{298}$[$(CH_3)_3COOH$].

C. Gas phase acidity of *tert*-butylhydroperoxide

We used phenylacetylene ($\Delta_{acid}G_{298}$[$C_6H_5C{\equiv}C$–H] $=362.9\ kcal\ mol^{-1}$) as a reference acid[40] in the establishment of the gas phase acidity of $(CH_3)_3COOH$ through measurement of proton transfer rate constants,

$$(CH_3)_3COOH+C_6H_5C{\equiv}C^- \rightleftharpoons (CH_3)_3COO^- + C_6H_5C{\equiv}CH. \quad (16)$$

The rate of proton transfer from *tert*-butyl hydroperoxide to phenyl acetylide anion (k_{16}) was measured to be 6.12 $(\pm 0.63)\times 10^{-10}\ cm^3\ molecule^{-1}\ s^{-1}$, and the reverse rate constant (k_{-16}) was found to be $8.50(\pm 0.18)\times 10^{-10}\ cm^3\ molecule^{-1}\ s^{-1}$. Therefore, *tert*-butyl hydroperoxide is $0.20\pm 0.07\ kcal\ mol^{-1}$ less acidic than phenylacetylene and its absolute gas phase acidity may be assigned as $363.1\ kcal\ mol^{-1}$. Collision induced dissociation of $(CH_3)_3COO^-$ was observed upon the injection of this ion into the reaction flow tube to produce HO_2^- and $(CH_3)_2C{=}CH_2$. However, the presence of HO_2^- (amounting to 10%–15% of the parent ion) does not affect the rate measurements of Eq. (16).

Benzyl alcohol, $(CH_3)_3CCH_2OH$, and $(CH_3)_3CCH(OH)CH_3$ were used as reference acids for measurement of $\Delta_{acid}G_{298}$[$(CH_3)_3COOH$] by Cooks' kinetic method and to verify the applicability of this approach for the systems studied. No products were observed in the CID spectra of the hydrogen bonded anion clusters other than the two anions competing for the proton. This is noteworthy in view of the fact that individual anions may be unstable towards elimination reactions even when injected at much lower kinetic energies. As noted above, $(CH_3)_3COO^-$ itself easily fragments to HO_2^- and *iso*-butylene $(CH_3)_2C{=}CH_2$. Similarly, benzyloxide $C_6H_5CH_2O^-$ decomposes upon injection to $C_6H_5^-$ and CH_2O. However, none of these fragment ions (HO_2^- or $C_6H_5^-$) were detected when clusters containing $(CH_3)_3COO^-$ or $C_6H_5CH_2O^-$ were subjected to collision-induced dissociation. We may conclude therefore that the process of dissociation of a cluster effectively dissipates the energy gained by collisions with the buffer gas, thus allowing for the survival of the component anions. Based on a calibration plot we found the coefficient α in Eq. (13) to be essentially unity in this flowing afterglow study, in line with our previous observations.[28]

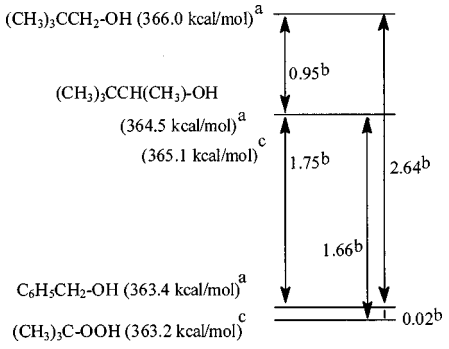

FIG. 6. The ladder of relative acidites of *tert*-butyl hydroperoxide and some alcohols. (a)$\Delta_{acid}G_{298}$/kcal mol^{-1} from Ref. 40. (b) Results of measurements by Cooks' kinetic method/kcal mol^{-1}; ± 0.2 kcal mol^{-1}. (c) $\Delta_{acid}G_{298}$, values determined in the present work.

The ladder of relative acidities obtained by the kinetic method is presented in Fig. 6 together with literature values[40] for the absolute acidities. Internal consistency of the ladder indicates that the kinetic method gives reliable values for the relative acidity of the compounds studied.

One should notice however that the relative acidity of 3,3-dimethylbutanol-2 [$(CH_3)_3CCH(OH)CH_3$] measured in this work disagrees with the literature value. This discrepancy prompted us to reexamine the absolute acidity of this compound using the thermodynamic method. We measured the rate constant for proton transfer from 3,3-dimethyl-butanol-2 to the anion[40] of acetonitrile ($\Delta_{acid}G_{298}$[CH_3CN]$=365.2\ kcal\ mol^{-1}$) (k_{17}) to be 9.07 $(\pm 0.30)\times 10^{-10}\ cm^3\ molecule^{-1}\ s^{-1}$ and for the reverse reaction $(k_{-17})=8.24(\pm 0.17)\times 10^{-10}\ cm^3\ molecule^{-1}\ s^{-1}$,

$$(CH_3)_3CCH(CH_3)OH+CH_2CN^- \rightleftharpoons (CH_3)_3CCH(CH_3)O^- + CH_3CN. \quad (17)$$

This indicates that this alcohol is $0.06\pm 0.03\ kcal\ mol^{-1}$ more acidic than acetonitrile and its absolute acidity may be assigned as $365.1\ kcal\ mol^{-1}$. This is $0.6\ kcal\ mol^{-1}$ higher than the literature value. Although this value is still within the stated[40] error bar ($\pm 2.0\ kcal\ mol^{-1}$), the correction is important as it makes the acidity ladder established in Fig. 6 consistent with the absolute acidity values and allows us to establish unequivocally the acidity of *tert*-butyl hydroperoxide from Cooks' kinetic method as $363.4\pm 0.2\ kcal\ mol^{-1}$. By averaging this value with that from the thermodynamic measurements ($363.1\pm 2.0\ kcal\ mol^{-1}$) we assign the gas phase acidity of *tert*-butyl hydroperoxide to be $\Delta_{acid}G_{298}$[$(CH_3)_3COO$–H]$=363.2\pm 2.0\ kcal\ mol^{-1}$.

IV. THERMOCHEMISTRY

Knowledge of $\Delta_{acid}G_{298}$[$(CH_3)_3COO$–H] and of the electron affinity of $(CH_3)_3COO$ allows us to calculate the bond enthalpy of *tert*-butyl hydroperoxide. Comparison with the bond enthalpies of hydrogen peroxide should indicate a trend common to peroxides. If one can measure the enthalpy of deprotonation for a species RH, [$\Delta_{acid}H_{298}$(RH)] and

TABLE V. Hydroperoxyl and *tert*-butylperoxyl radical energetics.

HO_2			Reference
EA($\tilde{X}\ ^2A''\ HO_2$)/eV	1.089 ± 0.006	(25.1 ± 0.1 kcal mol^{-1})	this work
$\Delta_{acid}H_{298}$(HOOH)/kcal mol^{-1}	376 ± 1		this work
Δ_fH_0(HOOH)/kcal mol^{-1}	-31.04 ± 0.05	$\Delta_fH_{298}=-32.48\pm0.05$	79
D_0(HOO–H)/kcal mol^{-1}	85.8 ± 0.6	$DH_{298}=87.1\pm0.6$	15
$\Delta_fH_0(HO_2)$/kcal mol^{-1}	4 ± 1	$\Delta_fH_{298}=3\pm1$	15
$T_0(\tilde{A}\ ^2A'\ HO_2)$/eV	0.871 574 5±0.000 000 2		34, 57
$T_0(\tilde{B}\ ^2A''\ HO_2)$/eV	5.9 ± 0.2		14, 4
IP(HO_2)/eV	11.352 ± 0.007		15, 51
$(CH_3)_3COO$			
EA[$\tilde{X}\ ^2A''(CH_3)_3COO$]/eV	1.196 ± 0.011	(27.6 ± 0.3 kcal mol^{-1})	this work
$\Delta_{acid}H_{298}[(CH_3)_3COO–H]$/kcal mol^{-1}	370.9 ± 2.0		this work
$D_0[(CH_3)_3COO–H]$/kcal mol^{-1}	83 ± 2	$DH_{298}=85\pm2$	this work
$\Delta_fH_{298}[(CH_3)_3COOH]$/kcal mol^{-1}	-58.8 ± 1.2		80
$\Delta_fH_{298}[(CH_3)_3COO]$/kcal mol^{-1}	-28 ± 2		this work
$\Delta_fH_{298}[(CH_3)_3COO]$/kcal mol^{-1}	-24.3 ± 2.2		45
$T_0[\tilde{A}\ ^2A'\ (CH_3)_3COO]$/eV	0.967 ± 0.011		this work
$T_0[\tilde{B}\ ^2A''(CH_3)_3COO]$/eV	5.2 ± 0.2		14, 4

separately find the electron affinity of the corresponding radical [EA(R)], then a simple cycle that uses the ionization potential of the H atom can provide a value for the bond enthalpy [DH_{298}(RH)],

$$\Delta_{acid}H_{298}(RH) = DH_{298}(RH)+IP(H)-EA(R) - \int_0^{298} dT[C_p(R)-C_p(R^-)+C_p(H)-C_p(H^+)]. \quad (18)$$

Since the sum of the integrated heat capacities is always[41] small ($\leqslant 0.3$ kcal mol^{-1}), the term in brackets can be ignored and we will use a more common expression, $\Delta_{acid}H_{298}(RH)\cong DH_{298}(RH)+IP(H)-EA(R)$.

The bond energies of hydrogen peroxide have been measured earlier[15] and are reported as $D_0(HOO–H)=86\pm1$ kcal mol^{-1} and $DH_{298}(HOO–H)=88\pm1$ kcal mol^{-1}. Because there are accurate values for the hydrogen peroxide bond enthalpy and the hydroperoxyl electron affinity is available, we can compute the value of the enthalpy of deprotonation of hydrogen peroxide more accurately than it has been measured,[41] $\Delta_{acid}H_{298}(H_2O_2)=DH_{298}(HOO–H)+IP(H)-EA(HO_2)$. We calculate $\Delta_{acid}H_{298}(H_2O_2)=376\pm1$ kcal mol^{-1} which overlaps the previously reported value.[20,21]

For $(CH_3)_3COOH$, the enthalpy of deprotonation must be calculated from the gas phase acidity, $\Delta_{acid}G_{298}[(CH_3)_3COOH]=363.2\pm2.0$ kcal mol^{-1}. Since $\Delta_{acid}G_{298}=\Delta_{acid}H_{298}-T\Delta_{acid}S_{298}$, a value of $\Delta_{acid}S_{298}$ must be found. One can use the calculated rotational constants[42] for *tert*-butyl hydroperoxide and *tert*-butyl hydroperoxyl anion to estimate $\Delta_{acid}S_{298}[(CH_3)_3COOH]=25.9$ cal mol^{-1} K^{-1}. Thus, $\Delta_{acid}H_{298}[(CH_3)_3COOH]=370.9\pm2.0$ kcal mol^{-1}. Use of the electron affinity, $EA[(CH_3)_3COO]=1.196\pm0.011$ eV, leads to a value for the bond enthalpy of *tert*-butyl hydroperoxide, $DH_{298}[(CH_3)_3COO–H]=85\pm2$ kcal mol^{-1}. The bond enthalpy at 298 K and the bond energy at 0 K are related by the heat capacities,

$$DH_{298}(RH)=D_0(RH)+\int_0^{298} dT[C_p(R)+C_p(H)-C_p(RH)]\cong D_0(RH)+\int_0^{298} dTC_p(H). \quad (19)$$

Since the integrated heat capacity for the H atom is $5/2RT$, we compute $D_0[(CH_3)_3COO–H]=83\pm2$ kcal mol^{-1}. These bond enthalpies[43] are 3 kcal mol^{-1} lower than those for H_2O_2. Table V summarizes the thermochemical parameters.

It is important to compare these findings to other measurements of the bond enthalpies of HO_2 and RO_2. Many calculations have been performed to estimate the bond dissociation energy. Using G2 theory,[44] estimates were found for D_0(HO–OH) (50 kcal mol^{-1}) and $D_0(CH_3O–OH)$ (45 kcal mol^{-1}). Slagle *et al.*[45] studied the equilibrium reaction of oxygen with alkyl radicals, $R+O_2\rightleftharpoons RO_2$. These studies measured the bond enthalpies for ethylperoxyl radical, $DH_{298}[CH_3CH_2–O_2]=35.2\pm1.5$ kcal mol^{-1}, and *tert*-butylperoxyl radical, $DH_{298}[(CH_3)_3C–O_2]=36.7\pm1.9$ kcal mol^{-1}; other less direct studies are available as well.[46] Table VI lists some bond dissociation reactions with enthalpies computed from the experimental heats of formation listed for comparison. We have also included the thermochemistry of alkylperoxyl radical oxidation of NO to NO_2 because of the importance of this process in tropospheric ozone formation.[5]

Ab initio complete basis set electronic structure calculations[47,48] using the GAUSSIAN 94 program[49] can successfully reproduce the experimental bond energies. Table VII lists the results of the CBS-Q calculations that we have performed for hydrogen peroxides and the three simplest alkylperoxides.

V. THERMOCHEMISTRY AND REARRANGEMENT MECHANISMS OF PEROXYL RADICALS

In this study we have refined the value of EA(HO_2). There are several measures of the ionization potential,

TABLE VI. (a) Thermochemistry of peroxyl radicals: Auxiliary heats of formation. (b) Reaction.

Species	$\Delta_f H_{298}$ /kcal mol^{-1}	$\Delta_f H_0$ /kcal mol^{-1}	Reference
(a)			
H	52.103±0.001	51.633±0.001	81
$O(^3P_2)$	59.55±0.02	58.98±0.02	81
H_2O	−57.795±0.010	−57.102±0.010	82
OH $X\ ^2\Pi$	9.40±0.05	9.34±0.05	81
NO $X\ ^2\Pi$	21.58±0.04	21.46±0.041	81
$NO_2\ \tilde{X}\ ^2A_1$	7.91±0.19	8.59±0.191	81
$O_3\ \tilde{X}\ ^1A_1$	33.9±0.5	34.5±0.5	82
$CH_2{=}CH_2$	12.52±0.12	14.56±0.12	82
$CH_3CH_2\ \tilde{X}\ ^2A'$	28.9±0.4	31.5±0.5	41
$CH(CH_3)_3$	−32.1±0.2	−25.3±0.3	83
$C(CH_3)_3\ \tilde{X}\ ^2A_2''$	12.3±0.4	18.1±0.6	77
$(CH_3)_2C{=}CH_2$	−4.0±0.1		83
$H_2C{=}O$	−25.98±0.12	−25.06±0.12	82
$HCO\ \tilde{X}\ ^2A'$	10.0±0.2	9.9±0.2	41
CH_3OH	−48.04±0.14	−45.42±0.14	82
$CH_3O\ \tilde{X}\ ^2E$	4.1±0.9	5.9±0.9	41
$CH_2OH\ \tilde{X}\ ^2A''$	−2.9±1.0	−4.4±1.0	41
CH_3CH_2OH	−56.12±0.12	−51.88±0.12	79
$CH_3CH_2O\ \tilde{X}\ ^2A''$	−3.7±0.8	−0.4±0.9	41
CH_3CHO	−39.7±0.1	−37.2±0.2	83
$CH_2CHO\ \tilde{X}\ ^2A''$	2.5±2.2	4.0±2.2	41
$CH_3CO\ \tilde{X}\ ^2A'$	−2.4±0.3	−0.9±0.3	41
H_2O_2	−32.48±0.05	−31.04±0.05	82
$HO_2\ \tilde{X}\ ^2A''$	3±1	4±1	15
$(CH_3)_3COOH$	−58.8±1.2		80
$(CH_3)_3COOH$	−59.0		84
$(CH_3)_3COO\ \tilde{X}\ ^2A''$	−24.3±2.2		45
CH_3OOH	−31.2	−33.9	85, 86
CH_3OOH	−32.3	−35.0	84, 86
$CH_3OO\ \tilde{X}\ ^2A''$	2.5±0.7	0.1±1.0	14, 86
CH_3CH_2OOH	−40.2±1.2	−43.7±1.4	84, 86
$CH_3CH_2OO\ \tilde{X}\ ^2A''$	−6.9±1.6	−10.0±1.8	14, 86

(b)		$\Delta_{rxn}H_{298}$ /kcal mol^{-1}
A1. HOOH	$\rightarrow HOO(^2A'')+H$	88±1
A2. HOOH	$\rightarrow HO(^2\Pi)+OH(^2\Pi)$	51.3± 0.1
A3. $HOO(^2A'')$	$\rightarrow HO(^2\Pi)+O(^3P)$	66±1
A4. $HOO(^2A'')$	$\rightarrow H+O_2(^3\Sigma_g^-)$	49±1
A5. $(CH_3)_3COOH$	$\rightarrow (CH_3)_3COO(^2A'')+H$	87±2
A6. $(CH_3)_3COOH$	$\rightarrow (CH_3)_3CO(^2E)+OH(^2\Pi)$	47±1
A7. $(CH_3)_3COOH$	$\rightarrow (CH_3)_3C(^2A_2'')+OOH(^2A'')$	74±2
A8. $(CH_3)_3COO(^2A'')$	$\rightarrow (CH_3)_3C(^2A_2'')+O_2(^3\Sigma_g^-)$	37±2
A9. $(CH_3)_3COO(^2A'')$	$\rightarrow (CH_3)_3CO(^2E)+O(^3P)$	63±2
A10. $(CH_3)_3COO(^2A'')$	$\rightarrow (CH_3)_2C{=}CH_2+OOH(^2A'')$	23±2
A11. CH_3OOH	$\rightarrow CH_3OO(^2A'')+H$	87±1
A12. CH_3OOH	$\rightarrow CH_3O(^2E)+OH(^2\Pi)$	46±1
A13. CH_3OOH	$\rightarrow CH_3(^2A_2'')+OOH(^2A'')$	70±1
A14. $CH_3OO(^2A'')$	$\rightarrow CH_3(^2A_2'')+O_2(^3\Sigma_g^-)$	32.5±0.7
A15. $CH_3OO(^2A'')$	$\rightarrow CH_3O(^2E)+O(^3P)$	61±1
A16. $CH_3OO(^2A'')$	$\rightarrow H_2C{=}O+OH(^2\Pi)$	−19.1±0.8
A17. CH_3CH_2OOH	$\rightarrow CH_3CH_2OO(^2A'')+H$	85±2
A18. CH_3CH_2OOH	$\rightarrow CH_3CH_2O(^2A'')+OH(^2\Pi)$	46±1
A19. CH_3CH_2OOH	$\rightarrow CH_3CH_2(^2A')+OOH(^2A'')$	72±1
A20. $CH_3CH_2OO(^2A'')$	$\rightarrow CH_3CH_2(^2A')+O_2(^3\Sigma_g^-)$	36±2
A21. $CH_3CH_2OO(^2A'')$	$\rightarrow CH_3CH_2O(^2A'')+O(^3P)$	63±2
A22. $CH_3CH_2OO(^2A'')$	$\rightarrow CH_3CHO+OH(^2\Pi)$	−23±2
A23. $CH_3CH_2OO(^2A'')$	$\rightarrow CH_2{=}CH_2+HOO(^2A'')$	22±2
A24. $CH_3O_2(^2A'')+NO(^2\Pi)$	$\rightarrow CH_3O(^2E)+NO_2$	−12±1
A25. $CH_3CH_2O_2(^2A'')+NO(^2\Pi)$	$\rightarrow CH_3CH_2O(^2A'')+NO_2$	−10±2
A26. $(CH_3)_3CO_2(^2A'')+NO(^2\Pi)$	$\rightarrow (CH_3)_3CO(^2E)+NO_2$	−10±2
A27. $CH_3O_2(^2A'')+O_3(^1A_1)$	$\rightarrow CH_3O(^2E)+2O_2$	−32±1
A28. $CH_3CH_2O_2(^2A'')+O_3(^1A_1)$	$\rightarrow CH_3CH_2O(^2A'')+2O_2$	−31±2
A29. $(CH_3)_3CO_2(^2A'')+O_3(^1A_1)$	$\rightarrow (CH_3)_3CO(^2E)+2O_2$	−30±2

TABLE VII. Complete basis set calculated bond dissociation energies/kcal mol^{-1}.

	CBS-Q	CBS/APNO	Expt D_0 (from Table VI)
D_0[HOO–H]	86.7±1.2	85.4±0.7	86±1
D_0[CH_3OO–H]	84.5±1.2	···	85±1
D_0[CH_3CH_2OO–H]	84.2±1.2	···	84±2
D_0[$(CH_3)_3$COO–H]	···	···	84±2
D_0[HO–OH]	49.2±1.2	48.6±0.7	49.7±0.1
D_0[CH_3O–OH]	44.2±1.2	···	44±1
D_0[CH_3CH_2O–OH]	44.0±1.2	···	44±2
D_0[$(CH_3)_3$CO–OH]	···	···	45±1
D_0[HO–O]	64.1±1.2	64.7±0.7	65±1
D_0[CH_3O–O]	61.4±1.2	···	60±2
D_0[CH_3CH_2O–O]	61.5±1.2	···	61±2
D_0[$(CH_3)_3$CO–O]	···	···	62±2

IP(HO_2). The bond energy and photoionization mass spectrometric appearance energy are related[41] through the ionization potential of the radical,

$$\mathrm{AP}(HO_2^+,H_2O_2)=D_0(\mathrm{HOO–H})+\mathrm{IP}(HO_2). \tag{20}$$

An older electron impact mass spectroscopy study[50] reported $\mathrm{AP}(HO_2^+,H_2O_2)=15.4\pm0.1$ eV and while a more recent value[51] is reported as $\mathrm{AP}(HO_2^+,H_2O_2)=15.12\pm0.02$ eV. The accurate value[15] for D_0(HOO–H) permitted the hydroperoxyl ionization potential to be extracted from $\mathrm{AP}(HO_2^+,H_2O_2)$ via Eq. (20) and it was found to be $\mathrm{IP}(HO_2)=11.40\pm0.03$ eV [or 11.7 ± 0.1 eV using the older appearance potential of Foner and Hudson]. The photoelectron spectrum of the hydroperoxyl radical has been reported[52] and photoionization produced HO_2^+ $\tilde{X}$ $^3A''$ with $\mathrm{IP}(HO_2)=11.35\pm0.01$ eV. The ionization potential for hydrogen peroxide itself, IP(H_2O_2), is poorly resolved[53] and is quoted as 11.69 eV while oxygen is listed[54] as $\mathrm{IP}(O_2)=12.071$ eV. This value for IP(HO_2) is striking since a heteroatom adjacent to a radical site generally lowers the IP appreciably. For example[55] IP(CD_3O) is 10.762 ± 0.008 eV and IP(CH_2OH) is 7.553 ± 0.006 eV. However there are reports[56] that IP[$(CH_3)_3$COOH] is 10.2 eV while[53] IP(CH_3OOCH_3) is 9.71 eV. So unlike the instance of the hydroxymethyl/methoxy radicals, in the case of hydrogen peroxide/hydroperoxyl radical, IP(H_2O_2) roughly equals IP(HO_2).

Following our detailed discussion of the spectroscopy and thermodynamics of the hydroperoxyl and *tert*-butylperoxyl radicals, HO_2 and $(CH_3)_3COO$, we turn our attention to (a) discussion of the available thermochemistry of the saturated alkylperoxyl radicals and (b) a novel mechanism for the rearrangements of saturated alkylperoxyl radicals (ROO) in combustion.

A. Alkylperoxyl radical thermochemistry

In Table VI, we have collected the most accurate thermochemistry for the RO_2 radicals that we are aware of. This table is arranged in two sections. The first section is a collection of auxiliary heats of formation of important species while the second section gives the reaction enthalpies of several important processes for RO_2 radicals.

From reactions (A1), (A5), (A11), and (A17), notice that the OH bond enthalpy, ROOH→RO_2+H, is about 85 kcal mol^{-1} while the OO bond enthalpy, ROOH→RO+OH, [(A2), (A6), (A12), and (A18)] is roughly 50 kcal mol^{-1}, as might be expected. Notice the peculiar fact that for the peroxyl radicals the ROO bond enthalpy, ROO→RO+O, is always about 63 kcal mol^{-1} [(A3), (A9), (A15), and (A21)]. Thus the bond enthalpy for the radical, RO–O, is *larger* than that for the hydroperoxide, RO–OH, by ~13 kcal mol^{-1}. This suggests that alkylperoxyl radicals (ROO) are likely to be more stable in a flame than the parent peroxide, ROOH.

In analogy with Eq. (7), one can make a reasonable conjecture about many of the important states of the alkylperoxyl radicals, cations, and anions; these are explicitly shown in expression (21). The GVB diagrams are compatible with the finding[37,57] of a ubiquitous RO_2 $\tilde{A}$ state of $^2A'$ symmetry in the near IR region of the electromagnetic spectrum at $T_e\cong7400$ cm^{-1}. Similarly (22) predicts that the electron affinity of the RO_2 radicals are universally higher than that of O_2. Charge transfer between O_2^- and RO_2 radicals is the basis of a chemical ionization mass spectrometric technique[7,8] for the monitoring of atmospheric alkylperoxyl radicals [$\mathrm{EA}(O_2)=0.451\pm0.007$ eV].[58] There is also a general, high lying $^2A''$ dissociative state[1] of the RO_2 radicals near 225–250 nm in the absorption spectrum,

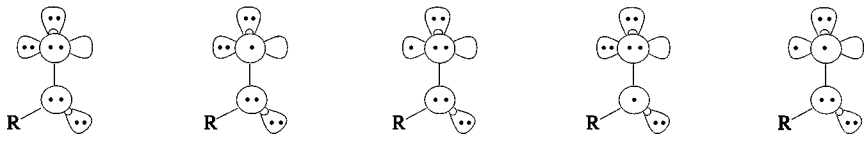

RO_2^- RO_2 RO_2 RO_2 RO_2^+

$\tilde{X}$ $^1A'\cong-1.0$ eV $\tilde{X}$ $^2A''=0$ eV $\tilde{A}$ $^2A'\cong1.0$ eV $\tilde{B}$ $^2A''\cong5.0$ eV $\tilde{X}$ $^3A''\cong11.2$ eV. (21)

B. Rearrangements of saturated alkylperoxyl radicals

The reaction of oxygen and alkyl radicals (or H atoms) is very exothermic, R+O_2+M→$RO_2(\tilde{X}\ ^2A'')$+M. For example it is exothermic [see (A4)] to form HO_2 from H+O_2 $^3\Sigma_g^-$ by 50 kcal mol^{-1}. The heat of reaction, R+O_2→RO_2, of some other

simple alkyl radicals can be taken from Table VI/kcal mol^{-1}: [CH_3, -32.5 ± 0.7], [CH_3CH_2, -36 ± 2], and [$(CH_3)_3C$, -37 ± 2]. The combination of oxygen with the alkyl radicals always leads to a 33–37 kcal mol^{-1} exothermic generation of alkylperoxyl radicals. The rate constants for the formation of these alkylperoxyl radicals are almost gas kinetic implying that $E_a[R+O_2\rightarrow RO_2]\cong 0$.

One of the intriguing reactions that peroxyl radicals undergo is an internal H atom abstraction followed by elimination.[3] A (1,5) elimination produces an alkene and the hydroperoxyl radical while a (1,4) process generates an aldehyde (or ketone) and hydroxyl,

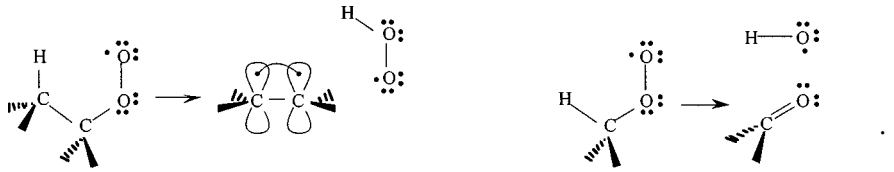

(1,5) Elimination (1,4) Elimination (22)

Table VI has the thermodynamics of (22). As (A16) and (A22) suggest, the (1,4) process is *exothermic* by $\sim$1 eV while the (1,5) rearrangement is *endothermic* by about 1 eV [(A23) and (A10)]. Since the alkylperoxyl radicals in (22) are produced in an exothermic manner by reaction of alkyl radicals with oxygen, the RO_2 radicals are likely to be chemically activated by $\sim$35 kcal mol^{-1} so both cyclic elimination reactions in (22) are thermodynamically accessible. Consider the reactions of (a) the methyl radical with oxygen [(1,4) elimination only], (b) *tert*-butyl radical with oxygen [(1,5) elimination only], and (c) the oxidation of the ethyl radical where both the (1,4) and (1,5) processes are possible. With the explicit inclusion of the 32 kcal mol^{-1} RO_2 chemical activation, the production of the (1,4) products [aldehydes and hydroxyl] is now exothermic by about 55 kcal mol^{-1} while the generation of (1,5) products [alkenes and hydroperoxyl] becomes exothermic by $\sim$15 kcal mol^{-1},

Reaction	$\Delta_{rxn}H_{298}$/kcal mol^{-1}	
$CH_3(^2A_2'')+O_2(^3\Sigma_g^-)\rightarrow CH_2{=}O+OH(^2\Pi)$	-52 ± 1,	(23a)
$(CH_3)_3C(^2A_2'')+O_2(^3\Sigma_g^-)\rightarrow (CH_3)_2C{=}CH_2+HO_2(^2A'')$	-14 ± 3,	(23b)
$CH_3CH_2(^2A')+O_2(^3\Sigma_g^-)\rightarrow CH_3CHO+OH(^2\Pi)$	-59 ± 2,	(23c)
$CH_3CH_2(^2A')+O_2(^3\Sigma_g^-)\rightarrow CH_2{=}CH_2+OOH(^2A'')$	-14 ± 2.	(23d)

We wish to suggest mechanisms for both the (1,4) and (1,5) rearrangements in (22). Our model features the interplay of the two low-lying electronic states of the peroxyl radical, RO_2 $\tilde{X}\ ^2A''$ and $\tilde{A}\ ^2A'$. We realize that vibronic coupling will ''mix'' these two electronic states somewhat, so the schemes that follow are only approximate. Nevertheless we believe that our mechanisms will be valuable to help understand the framework underpinning the reactivity of peroxyl radicals.

The (1,4) RO_2 cyclic elimination commences with the combination of R and oxygen to produce the $^2A''$ ground state of RO_2 which is ''chemically activated'' by approximately 32 kcal mol^{-1} [see (A14)]; the activated complex in (24) is indicated by $[CH_3O_2]^{\dagger}$. One could write a mechanism for this reaction as an internal proton transfer,

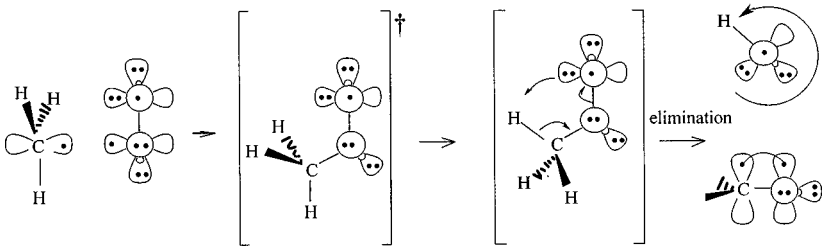

(24)

What would be the activation barrier for (24)? This has not been measured but the thermal elimination of hydrochloric acid from chloroethane is a comparable six-electron process, $CH_3CH_2Cl+\Delta\rightarrow CH_2{=}CH_2+HCl$. The barrier for elimination of HCl from ethylchloride has been reported[59] to be $E_a=58.4\pm1.5$ kcal mol^{-1} while if CD_2HCD_2Cl is the substrate,[60] $E_a=54.0\pm1.2$ kcal mol^{-1}. Consequently the activation energy for the proton transfer mechanism in (24) is roughly 50–60 kcal mol^{-1}.

Rather than an ''ionic mechanism,'' Eq. (24), one could consider a ''radical process'' that features internal abstraction of a H atom rather than a proton. However the unpaired electron in RO_2 $^2A''$ is poorly aligned to abstract the neighboring H atom. A more ''reactive'' configuration of RO_2 will be $\tilde{A}^2A'$. As Eq. (21) suggests, excitation to the $\tilde{A}^2A'$ configuration requires roughly 20 kcal mol^{-1},

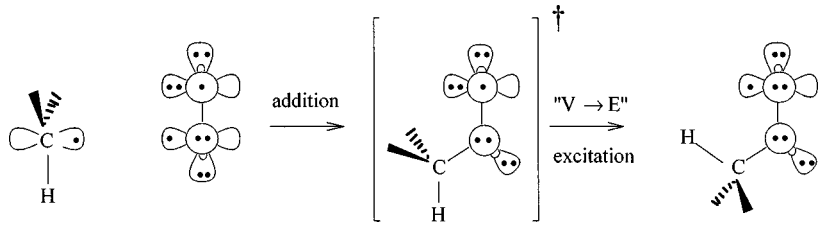

$\tilde{X}^2A''$ $\tilde{A}^2A'$ (25)

The $\tilde{A}^2A'$ configuration is a different electronic state than the ground state. The ''$V \rightarrow E$'' process in (25) has all the appearances of a ''reverse internal conversion'' and is unprecedented. Alternatively one could argue that the initial collision complex of R with O_2 undergoes a curve-crossing and produces the excited alkylperoxyl radical, RO_2 $\tilde{A}$ $^2A'$. For a (1,4) elimination, the activated $\tilde{A}$ $^2A'$ state should have an additional cyclization barrier (making a four-membered ''ring'') to surmount before eliminating OH and producing the aldehyde/ketone in Eq. (26),

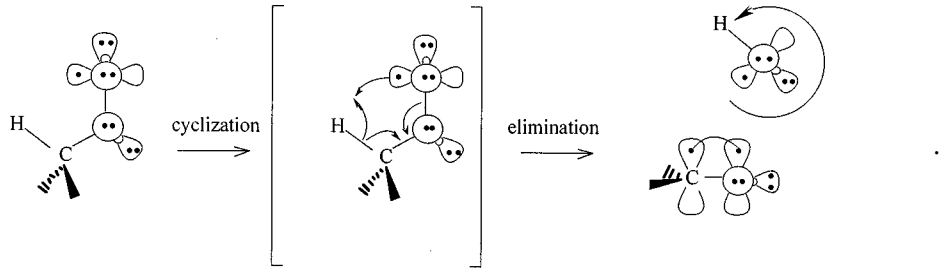

$\tilde{A}$ $^2A'$ (26)

We estimate[61,62] the cyclization barrier to be roughly 15 kcal mol^{-1} so if the ''$V \rightarrow E$'' and cyclization energies are ''additive,'' the barrier to (1,4) cyclization will be roughly 1.5 eV or $E_a(1,4) \cong 35$ kcal mol^{-1}.

Experimental evidence for collisional formation of the $\tilde{A}$ $^2A'$ state of peroxyl radicals exists. The excited electronic state of HO_2 has been observed following thermal addition of H to O_2 in a fast flow reactor.[63] These experiments clearly detected near-IR chemiluminescence from HO_2 $\tilde{A}$ $^2A'$ ($\nu_3 \leqslant 6$) formed by the titration of H atoms with O_2; HO_2 $\tilde{A}$ $^2A' \rightarrow HO_2$ $\tilde{X}$ $^2A''$. Since the RO_2 radicals have many similarities to the hydroperoxyl radical, the chemiexcitation of hydroperoxyl radicals at room temperature implies that energy transfer processes might form RO_2 $\tilde{A}$ $^2A'$ following addition of R to O_2. Since HO_2 $\tilde{A}$ $^2A'$ is such a small molecule and cannot rearrange, chemiluminescence of near-IR photons is an important route to the hydroperoxyl radical ground state. Shock tube studies[64] of the reaction of CH_3 radicals with O_2 have provided some information about the properties of CH_3O_2. At temperatures above 1500 K, the decomposition of the methylperoxyl radical to O and OH were observed. It was reported[64] that the activation energy for the production of OH from CH_3+O_2 was fit to $E_a(23a) = 251$ kJ mol^{-1} (60 kcal mol^{-1}). If the ''chemically activated'' CH_3O_2 $\tilde{A}$ $^2A'$ configuration decomposes in a direct manner as in Eq. (26), the product OH radical will emerge rotating in the plane of the hydrocarbon. Such a mechanism should preferentially populate only one of the two possible Λ doublet states of OH ($^2\Pi$).

The dynamics of a (1,5) HO_2 elimination from an organic peroxyl radicals will be similar to (1,4) OH elimination process. Reaction of the alkyl radical with O_2 will produce a RO_2 $^2A''$ species that is chemically activated by about 32 kcal mol^{-1} [see Eq. (21)]. A synchronous proton transfer reaction by analogy to (26), will produce an alkene and the HO_2 radical. But a six-electron electrocyclic process produces HO_2 in the excited state, $\tilde{B}$ $^2A''$, *not* the ground state, $\tilde{X}$ $^2A''$,

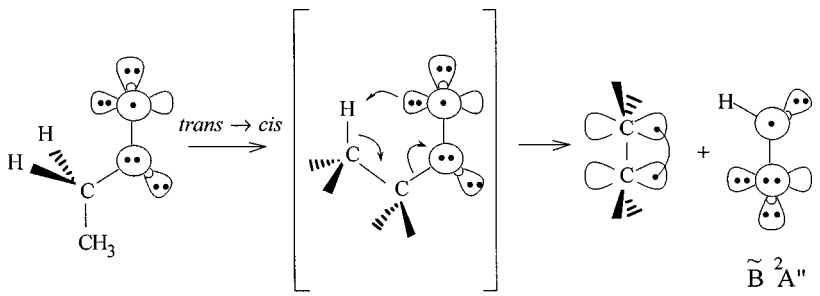

$\tilde{B}$ $^2A''$ (27)

From Table V the excited state of HO_2 is nearly 136 kcal mol^{-1} above the ground state; $T_0(\tilde{B}\ ^2A''\ HO_2) = 5.9 \pm 0.2$ eV.

Rather than a proton transfer mechanism, a radical process can generate HO_2 and an alkene via a hydrogen atom transfer. As with the case of the (1,4) rearrangement, a H atom transfer would most likely involve the excited, $\tilde{A}\ ^2A'$ state of the RO_2 radical. To populate the $RO_2\ \tilde{A}\ ^2A'$ state the $\tilde{X}$ RO_2 radical undergoes a ''$V \rightarrow E$'' energy transfer following its formation or, perhaps, the RO_2 radical suffers a curve-crossing on the initial O_2/radical collision,

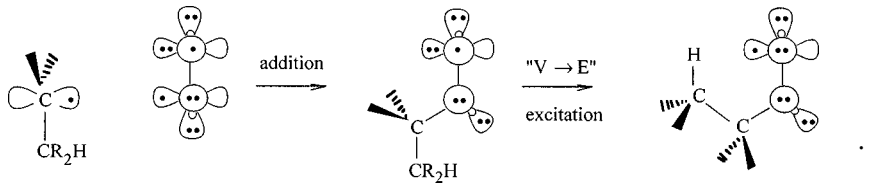

$\tilde{X}\ ^2A''$ $\tilde{A}\ ^2A'$ (28)

The activation energy required to close to a five-membered activated complex will be small.[61,62] However if the activated complex has a plane of symmetry and if the subsequent abstraction is a ''direct process'' [no intermediate between the $RO_2\ \tilde{A}\ ^2A'$ configuration and the (alkene, HO_2) products that lasts several rotational periods], then the product hydroperoxyl radical will be produced in an excited state, $HO_2\ \tilde{A}\ ^2A'$. The thermodynamics of (1,5) cyclizations exclude this ''direct process'' because the production of $HO_2\ \tilde{A}\ ^2A'$ from $CH_3CH_2 + O_2$ radicals is endothermic by approximately 5 kcal mol^{-1} [see (23d)],

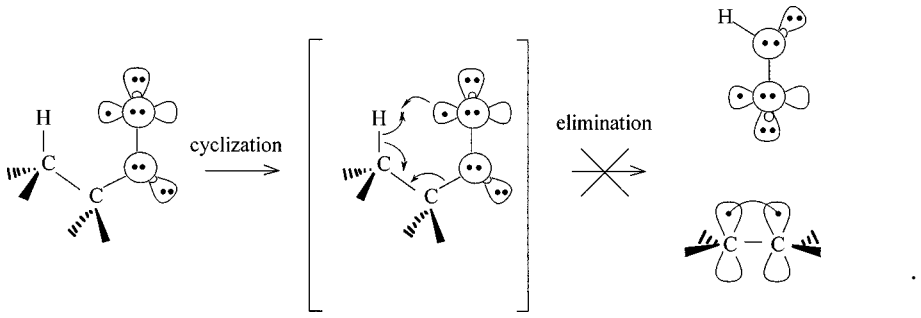

$\tilde{A}\ ^2A'$ $HO_2\ \tilde{A}\ ^2A'$ (29)

This suggests the presence of a curve crossing along the ''direct'' (1,5) cyclization path. Excitation of a nonsymmetric vibrational mode such as an a'' distortion could break the planar symmetry of the activated process so the activated complex is vibronically of $^2A''$ symmetry. Such a Herzberg–Teller-type coupling formally enables production of $HO_2\ \tilde{X}\ ^2A''$.

Alternatively, the cyclization might not be a ''direct'' process but proceed through a discrete intermediate (a species with a lifetime of several rotational periods). As an example, the stepwise abstraction of a tertiary H by oxygen to produce a hydroperoxyl radical would cost[65] $\sim$15 kcal mol^{-1}. The chemically activated RO_2 species probably has just enough energy to accomplish this abstraction, shown in (30),

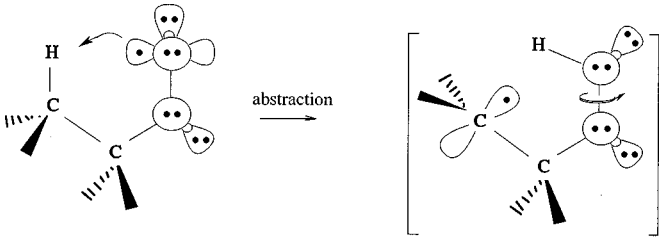

(30)

By analogy[66] with the twisted equilibrium structure for H_2O_2, formation of a carbon-centered hydroperoxyl radical such as (30) will be followed by rapid relaxation about the RO–OH torsional angle. This torsional motion will break the planar symmetry and the complex can disintegrate as in (31) with the expulsion of $HO_2\ \tilde{X}\ ^2A''$ from the alkene,

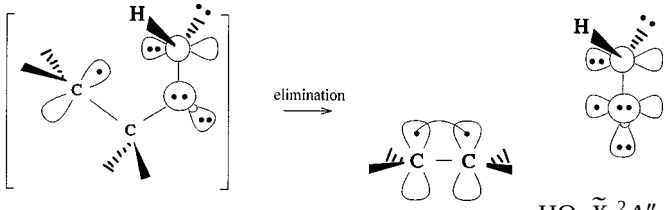

$HO_2\ \tilde{X}\ ^2A''$ (31)

It is not simple to anticipate the dynamical path that will be followed by the chemically activated RO_2 adduct along the (1,5) elimination as it traverses the [$RO_2\ \tilde{X}\ ^2A'' \rightarrow RO_2\ \tilde{A}\ ^2A' \rightarrow$ olefin + HO_2] path.

Interestingly, the reaction dynamics are much less of a constraint for the peroxide anions (ROO^-) in contrast to the peroxyl radicals since the ions have a closed-shell electronic configuration. Recall (*vide supra*) that we easily observed the

collision-induced rearrangement of the *tert*-butylperoxide anion in the FA/SIFT apparatus to produce the hydroperoxide anion $(CH_3)_3COO^- + He \rightarrow H_2C{=}C(CH_3)_2 + HO_2^- + He$,

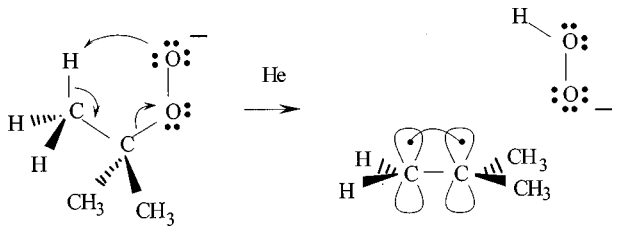

(32)

These proposed mechanisms for peroxyl radical fragmentation in (24)–(29) are in accord with most of the published alkyl peroxide findings. The initial radical/radical addition, $R + O_2$, has been observed.[45] At temperatures up to 300 °C, an equilibrium of $R + O_2 \rightleftharpoons RO_2$ is observed with only small concentrations of alkylperoxyl radicals. The decomposition of the organic peroxyl radicals is known to lead to several products depending on pressure and temperature. Above 400 °C this equilibrium is shifted to the right and the RO_2 can form either aldehydes/ketones together with OH (1,4 abstraction), or produce alkenes and HO_2 radicals (1,5 abstraction).[67]

Many *ab initio* electronic structure calculations have been reported for $CH_3 + O_2$. Jursic[68] used DFT methods to calculate a barrier of 40–44 kcal mol^{-1} for CH_3O_2 to rearrange to form $CH_2{=}O + OH$, and 30–40 kcal mol^{-1} to produce $CH_3O + O$. *Ab initio* calculations by Saito *et al.*[69] show a transition state for the OH forming reaction that is 49.2 kcal mol^{-1} above the CH_3O_2 adduct which requires an electronically excited transition state. Walch[70] performed CASSCF/CI calculations on the methylperoxyl reaction pathway and found no barrier for adduct formation, $CH_3 + O_2 \rightarrow CH_3O_2$. A barrier of 13.7 kcal mol^{-1} was computed on the $\tilde{A}\ ^2A'$ surface (19.7 kcal mol^{-1} above the $\tilde{X}\ ^2A''$ surface) leading to the exothermic formation of $CH_2O + OH$. The $\tilde{X}\ ^2A''$ surface leads to the formation of $CH_3O + O$, 26.2 kcal mol^{-1} above the initial reactants. However, if the C_S symmetry is broken (by a methyl rotation, for example), the CH_3O_2 could follow a minimum energy pathway to $CH_2O + OH$ with the largest calculated barrier above the reactants by 13.7 kcal mol^{-1}. The nature of the barrier to the chemically activated transition state, $CH_3O_2^*$, has been examined. Considerations of the estimate of ring strain[3] and methyl and ethyl rotational barriers[68,71] that could break symmetry have been examined.

The reaction $C_2H_5 + O_2 \rightarrow C_2H_4 + HO_2$ has been experimentally studied several times.[2,72] A combined experimental/modeling study[72] concluded that direct H abstraction from CH_3CH_2 by O_2 is a minor channel above 1000 K, and is not a major pathway at lower temperatures. Slagle, Feng, and Gutman[67] have proposed a pathway for the reaction of ethyl radical with oxygen, $CH_3CH_2 + O_2 \rightarrow CH_3CH_2O_2 \rightarrow$ [ring structure] $\rightarrow CH_2CH_2OOH \rightarrow C_2H_4 + HO_2$. This mechanism is similar to Eqs. (30) and (31) and has no barriers above the energy of the reactants. The estimate of the barrier

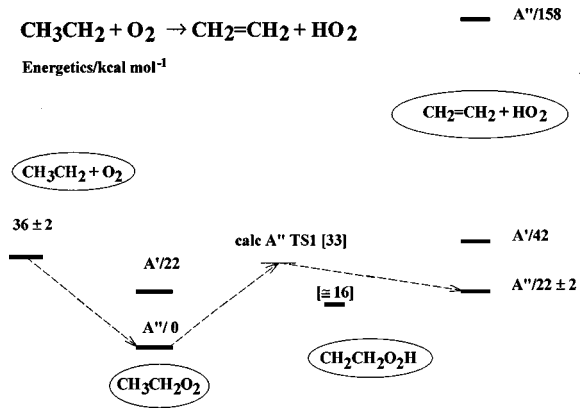

FIG. 7. The experimental energetics of the reduction of oxygen by the ethyl radical, $CH_3CH_2 + O_2 \rightarrow CH_2{=}CH_2 + HO_2$ /kcal mol^{-1}. We estimate the energy of the CH_2CH_2OOH radical to be roughly 16 kcal mol^{-1} above that of the $CH_3CH_2O_2$ radical. The $^2A''$ transition state, TS1, is calculated by Ignatyev *et al.* to be 33 kcal mol^{-1} above that of the $CH_3CH_2O_2$ radical.

from $CH_3CH_2O_2 \rightarrow$[(1,5) ring] of 23 kcal mol^{-1} is very similar to the $[\tilde{A}\ ^2A' \leftarrow \tilde{X}\ ^2A'']$ energy proposed in (29). RRKM theory was used[72] to interpret the experimental rate constants for $CH_3CH_2 + O_2$ to construct a more detailed reaction path consistent with the high temperature behavior of the reaction. This model shows that the ethyl radical and oxygen have no barrier to formation of the adduct, $CH_3CH_2O_2$.

The oxidation of alkyl radicals by molecular oxygen has been theoretically studied several times.[71,73,74] These three papers provide a nice summary of the experimental findings for the simplest reaction, $O_2 + CH_3CH_2 \rightarrow H_2C{=}CH_2 + HO_2$. Ignatyev *et al.*[74] identified three general pathways for the reaction of ethyl radical with molecular oxygen; (a) formation of $CH_3CH_2O_2$ followed by concerted elimination of ethylene; (b) formation of $CH_3CH_2O_2$ followed by rearrangement to CH_2CH_2OOH and then elimination of ethylene; and (c) direct H atom abstraction by O_2.

Pathway (c) is the direct abstraction of $CH_2CH_2{-}H$ by O_2 and is believed to be a minor pathway. The activated complex for this direct process was located by carrying out *ab initio* electronic structure, B3LYP/TZ2Pf, calculations. The transition state for (33), TS1′($^2A''$), was located 13.5 kcal mol^{-1} above the energy of the reactant O_2 and CH_3CH_2,

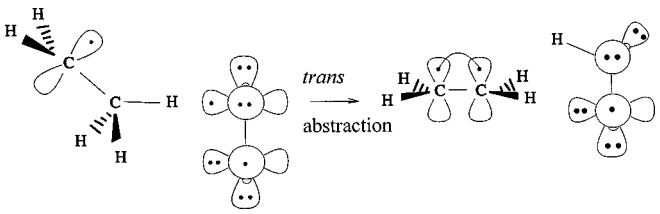

$CH_3CH_2\ ^2A''$ $O_2\ ^3\Sigma_g^-$ $\tilde{X}\ ^1A_1$ $HO_2\tilde{X}\ ^2A''$

(33)

Pathway (a) is the concerted elimination route; the activated complex for HO_2 elimination [TS1 ($^2A''$)] was computed[74] to be 3 kcal mol^{-1} below starting materials,

$CH_3CH_2+O_2$. Using the experimental values from Table VI, we have sketched the important intermediates in Fig. 7 for the $CH_3CH_2O_2 \rightarrow CH_2{=}CH_2+HO_2$ reaction. We estimate[65] the energy of the CH_2CH_2OOH radical to be approximately 16 kcal mol^{-1} above the $CH_3CH_2O_2$ radical and Fig. 7 displays the lowest transition state [TS1 $^2A''$] calculated[74] for the concerted elimination of ethylene and HO_2. The lowest energy pathway for $CH_3CH_2O_2 \rightarrow CH_2{=}CH_2+HO_2$ is traced by the dashed line. Pathway (b) describes the sequential process, $CH_3CH_2O_2 \rightarrow CH_2CH_2OOH \rightarrow CH_2{=}CH_2+O_2H$. The transition state for rearrangement of ethyperoxyl radical to the hydroperoxyethyl radical was computed[74] to be TS2(^2A)8.0 kcal mol^{-1} above $CH_3CH_2+O_2$. The symmetry of this transition state was broken from C_s to C_1.

We suggest that there are two parallel mechanisms for the oxidation of the ethyl radical by O_2. (a) If CH_3CH_2 and O_2 combine to produce the ground state $CH_3CH_2O_2$ radical, $\tilde{X}\ ^2A''$, then the reactive trajectories will follow a ''proton transfer'' pathway reminiscent of (27) and the activated complex will be described by Ignatyev *et al.*'s TS1. This $^2A''$ proton transfer might be described by

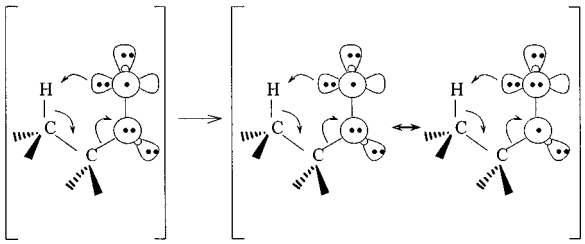

$$\Psi = \psi_{\mathrm{I}}[\mathrm{EtO_2}/^2A''] \qquad \Psi = \psi_{\mathrm{I}}[\mathrm{EtO_2}/^2A''] + \psi_{\mathrm{II}}[\mathrm{EtO_2}/^2A''] \tag{34a}$$

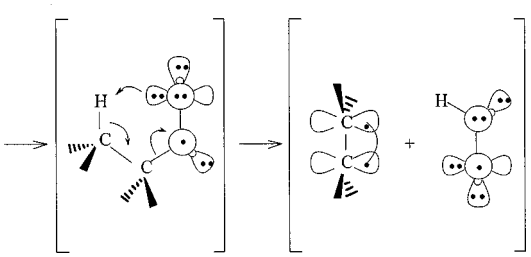

$$\psi_{\mathrm{II}}[\mathrm{EtO_2}/^2A''] \qquad \Psi = \psi[\mathrm{CH_2CH_2}/^1A_{1g}] + \psi[\mathrm{HO_2}/^2A''] \tag{34b}$$

The reaction starts with the *cis*-ethylperoxyl radical which is largely described by a single configuration, $\Psi = \psi_{\mathrm{I}}[\mathrm{EtO_2}/^2A'']$. As the reactive trajectory approaches the critical configuration, TS1, the system now must involve configuration mixing that includes an excited species, $^2A''$: $\Psi = c_{\mathrm{I}}\psi_{\mathrm{I}}[\mathrm{EtO_2}/^2A''] + c_{\mathrm{II}}\psi_{\mathrm{II}}[\mathrm{EtO_2}/^2A'']$. Passing through the critical configuration, TS1, the products are increasingly described by $\psi_{\mathrm{II}}[\mathrm{EtO_2}/^2A'']$ which evolves into the proper reaction products, $\psi[\mathrm{CH_2CH_2}/^1A_{1g}] + \psi[\mathrm{HO_2}/^2A'']$.

(b) Rather than a proton transfer, the peroxyl radical could rearrange by an internal H atom abstraction. A planar geometry is not likely for $\tilde{X}\ ^2A''$ $CH_3CH_2O_2$ to transfer a H atom from carbon to oxygen because the ''radical electron'' occupies an a'' orbital. Orbitals of a'' symmetry have a node in the molecular plane and will not overlap with the proximal H atom that sits in the plane. Consequently the reactive trajectory will come to a critical configuration, TS2, in which the C_s symmetry has been broken, (35). As overlap of the H atom with the a'' orbital grows an O–H bond will be formed and the C–H bond broken. The atom transfer will have an activation energy[65] of at least 15 kcal mol^{-1}

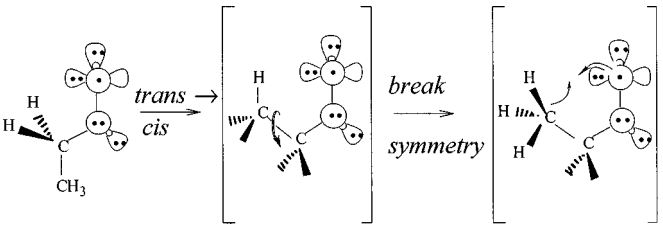

$$\Psi = \psi_{\mathrm{I}}[\mathrm{EtO_2}/^2A''] \qquad \Psi = \psi[\mathrm{EtO_2}/^2A] \tag{35}$$

The atom transfer produces the ethylhydroperoxyl radical, CH_2CH_2OOH, which recovers C_s symmetry and decomposes to $CH_2{=}CH_2+HO_2$ $\tilde{X}\ ^2A''$ via β scission, (36).

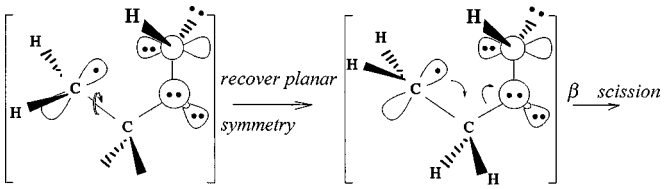

(36)

ACKNOWLEDGMENTS

G.B.E. is supported by a grant from the Chemical Physics Program, United States Department of Energy (DE-FG02-87ER13695). The National Science Foundation is gratefully acknowledged for support to W.C.L. (CHE97-03486 and PHY95-12150), C.H.D. (CHE-9421756) and V.M.B. (CHE-9734867). The GAUSSIAN 94 *ab initio* electronic structure calculations were carried out with a cluster of RSC-6000 digital computers supported by NSF CHE-9412767. We acknowledge Dr. Roberto Bianco and Dr. Larry Harding for some insightful discussions about peroxyl radical rearrangements. We thank Dr. G. A. Petersson for his theoretical support with the CBS calculations. Acknowledgment is made to the Donors of the Petroleum Research Fund administered by the American Chemical Society, for partial support of this research via PRF 30676-AC6. We thank Dr. A. R. Ravishankara and Dr. C. J. Howard for help with the purification of H_2O_2 and for some perspectives about alkylperoxyl radicals in the atmosphere. We have also benefited from discussions of Dr. V. Vaida and Dr. R. R. Fall about the ubiquitous presence of peroxyl radicals in the environment.

[1] P. D. Lightfoot, R. A. Cox, J. N. Crowley, M. Destriau, G. D. Hayman, M. E. Jenkin, G. K. Moortgat, and F. Zabel, Atmos. Environ., Part A **26**, 1805 (1992).

[2] A. C. Baldwin, in *The Chemistry of Peroxides*, edited by S. Patai (Wiley, New York, 1983), p. 97.

[3] A. Fish, in *Organic Peroxides*, edited by D. Swern (Wiley–Interscience, New York, 1970), Vol. 1.
[4] T. J. Wallington, P. Dagaut, and M. J. Kurylo, Chem. Rev. **92**, 667 (1992).
[5] F. Kirchner and W. R. Stockwell, J. Geophys. Res. **101**, 21007 (1996).
[6] B. J. Finlayson-Pitts and J. N. Pitts Jr., Science **276**, 1045 (1997).
[7] J. Eberhard, P. W. Willalta, and C. J. Howard, J. Phys. Chem. **100**, 993 (1996).
[8] J. Eberhard and C. J. Howard, J. Phys. Chem. **101**, 3360 (1997).
[9] C. K. Westbrook, Chem. Industry **100**, 562 (1992).
[10] B. K. Carpenter, J. Am. Chem. Soc. **115**, 9806 (1993).
[11] B. K. Carpenter, J. Phys. Chem. **99**, 9801 (1995).
[12] A. M. Mebel, E. W. G. Diau, M. C. Lin, and K. Morokuma, J. Am. Chem. Soc. **118**, 9759 (1996).
[13] A. Fahr, A. H. Laufer, M. Krauss, and R. Osman, J. Phys. Chem. **101**, 4879 (1997).
[14] P. D. Lightfoot, R. A. Cox, J. N. Crowley, M. Destriau, G. D. Hayman, M. E. Jenkin, G. K. Moortgat, and F. Zabel, Atmos. Environ., Part A **26**, 1805 (1992).
[15] C. J. Howard, J. Am. Chem. Soc. **102**, 6937 (1980).
[16] B. J. Moss and W. A. Goddard III, J. Chem. Phys. **63**, 3523 (1975).
[17] R. A. Bair and W. A. Goddard III, J. Am. Chem. Soc. **104**, 2719 (1982).
[18] W. A. Goddard III and L. B. Harding, Annu. Rev. Phys. Chem. **29**, 363 (1978).
[19] J. E. Bartmess and R. T. McIver, in *Gas Phase Ion Chemistry*, edited by M. T. Bowers (Academic, New York, 1979), Vol. 2, p. 87.
[20] V. M. Bierbaum, R. J. Schmitt, C. H. DePuy, R. D. Mead, P. A. Schulz, and W. C. Lineberger, J. Am. Chem. Soc. **103**, 6262 (1981).
[21] J. M. Oakes, L. B. Harding, and G. B. Ellison, J. Chem. Phys. **83**, 5400 (1985).
[22] K. M. Ervin and W. C. Lineberger, in *Gas Phase Ion Chemistry*, edited by N. G. Adams and L. M. Babcock (JAI, Greenwich, 1992), Vol. 1, p. 121.
[23] D. M. Neumark, K. R. Lykke, T. Andersen, and W. C. Lineberger, Phys. Rev. A **32**, 1890 (1985). $EA(O)=11\,784.645\pm0.006$ cm^{-1} or 1.461 110 $\pm0.000\,001$ eV.
[24] M. W. Siegel, R. J. Celotta, J. L. Hall, J. Levine, and R. A. Bennett, Phys. Rev. A **6**, 607 (1972).
[25] J. M. Van Doren, S. E. Barlow, C. H. DePuy, and V. M. Bierbaum, Int. J. Mass Spectrom. Ion Processes **81**, 85 (1987).
[26] M. S. Robinson, M. L. Polak, V. M. Bierbaum, C. H. DePuy, and W. C. Lineberger, J. Am. Chem. Soc. **117**, 6766 (1995).
[27] R. G. Cooks, J. S. Patrick, T. Kotiaho, and S. A. McLuckey, Mass Spectrom. Rev. **13**, 287 (1994).
[28] T. T. Dang, E. L. Motell, M. J. Travers, E. P. Clifford, G. B. Ellison, C. H. DePuy, and V. M. Bierbaum, Int. J. Mass Spectrom. Ion Processes **123**, 171 (1993).
[29] S. H. I. Hoke, S. S. Yang, R. G. Cooks, D. A. Hrovat, and W. T. Borden, J. Am. Chem. Soc. **116**, 4888 (1994).
[30] P. C. Engelking, J. Phys. Chem. **90**, 4544 (1986).
[31] C. T. Wickham-Jones, K. M. Ervin, G. B. Ellison, and W. C. Lineberger, J. Chem. Phys. **91**, 2762 (1989).
[32] M. E. Jacox, J. Phys. Chem. Ref. Data Monograph No. 3 (1994).
[33] K. H. Becker, E. H. Fink, P. Langen, and U. Schurath, J. Chem. Phys. **60**, 4623 (1974).
[34] R. P. Tuckett, P. A. Freedman, and W. J. Jones, Mol. Phys. **37**, 379 (1979).
[35] R. P. Tuckett, P. A. Freedman, and W. J. Jones, Mol. Phys. **37**, 403 (1979).
[36] G. Chettur and A. Snelson, J. Phys. Chem. **91**, 5873 (1987).
[37] J. E. Hunziker and H. R. Wendt, J. Chem. Phys. **64**, 3488 (1976).
[38] R. F. Gunion, Ph.D. thesis, University of Colorado, 1995.
[39] J. Cooper and R. N. Zare, J. Chem. Phys. **48**, 942 (1968).
[40] J. E. Bartmess, J. A. Scott, and R. T. McIver, J. Am. Chem. Soc. **101**, 6046 (1979).
[41] J. Berkowitz, G. B. Ellison, and D. Gutman, J. Phys. Chem. **98**, 2744 (1994).
[42] G. E. Davico, V. M. Bierbaum, C. H. DePuy, G. B. Ellison, and R. R. Squires, J. Am. Chem. Soc. **117**, 2590 (1995).
[43] S. P. Heneghan and S. W. Benson, Int. J. Chem. Kinet. **15**, 815 (1983).
[44] R. D. Bach, P. Y. Ayala, and H. B. Schlegel, J. Am. Chem. Soc. **118**, 12758 (1996).
[45] I. R. Slagle, E. Ratajczak, and D. Gutman, J. Phys. Chem. **90**, 402 (1986); V. D. Knyazev and I. R. Slagle, J. Phys. Chem. A **102,** 1770 (1998).
[46] K. A. Sahetchian, R. Rigny, J. T. De Maleissye, L. Batt, M. A. Khan, and S. Mathews, *Twenty-Fourth Symposium (International) on Combustion*, p. 637 (1992).
[47] J. W. Ochterski, G. A. Petersson, and J. A. Montgomery, Jr., J. Chem. Phys. **104**, 2598 (1996).
[48] J. A. Montgomery Jr., J. W. Ochterski, and G. A. Petersson, J. Chem. Phys. **101**, 5900 (1994).
[49] M. J. Frisch, G. W. Trucks, H. B. Schlegel, P. M. W. Gill, B. G. Johnson, M. A. Robb, J. R. Cheeseman, T. Keith, G. A. Petersson, J. A. Montgomery, K. Raghavachari, M. A. Al-Laham, V. G. Zakrzewski, J. V. Ortiz, J. B. Foresman, J. Cioslowski, B. B. Stefanov, A. Nanayakkara, M. Challacombe, C. Y. Peng, P. Y. Ayala, W. Chen, M. W. Wong, J. L. Andres, E. S. Replogle, R. Gomperts, R. L. Martin, D. J. Fox, J. S. Binkley, D. J. Defrees, J. Baker, J. P. Stewart, M. Head-Gordon, C. Gonzalez, and J. A. Pople, GAUSSIAN 94, Revision C2, 1996.
[50] S. N. Foner and R. L. Hudson, J. Chem. Phys. **36**, 2681 (1962).
[51] K. E. McCulloh, in *Proceedings of the 25th ASMS Conference on Mass Spectroscopy and Allied Topics* (Washington, D.C., 1977), p. 491. *Note added in proof:* M. Litorja and B. Rusic have recently measured $IP(HO_2)=11.352\pm0.007$ eV and $D_0(HO_2-H)=86.8\pm0.8$ kcal mol^{-1} (J. Electron Spectrosc. Relat. Phenom., in press).
[52] J. M. Dyke, N. B. H. Jonathan, A. Morris, and M. J. Winters, Mol. Phys. **44**, 1059 (1981).
[53] K. Kimura, S. Katsumata, Y. Achiba, T. Yamazaki, and S. Iwata, *Handbook of He I Photoelectron Spectra of Fundamental Organic Molecules* (Halsted, New York, 1981).
[54] K. P. Huber and G. Herzberg, *Constants of Diatomic Molecules* (Van Nostrand Reinhold, New York, 1979).
[55] B. Ruscic and J. Berkowitz, J. Chem. Phys. **95**, 4033 (1991). See, also the 202nd National Meeting, American Chemical Society, Division of Fuel Chemistry Symposium, New York, preprints of papers Vol. 36, 1571 (1991).
[56] C. Batich and W. Adam, Tetrahedron Lett. **16**, 1467 (1974).
[57] H. E. Hunziker and H. R. Wendt, J. Chem. Phys. **60**, 4622 (1974).
[58] M. J. Travers, D. C. Cowles, and G. B. Ellison, Chem. Phys. Lett. **164**, 449 (1989).
[59] K. A. Holbrook and A. R. W. Marsh, Trans. Faraday Soc. **63**, 643 (1967).
[60] C. J. Choi, B.-W. Lee, K.-H. Jung, and E. Tschuikow-Roux, J. Phys. Chem. **98**, 1139 (1993).
[61] J. D. Roberts and M. C. Caserio, *Basic Principles of Organic Chemistry* (Benjamin, Menlo Park, 1977), Table 12-3, p. 464.
[62] M. Jones Jr., *Organic Chemistry* (Norton, New York, 1997), Table 6.2 in Sec. 6.1.
[63] K. J. Holstein, E. H. Fink, J. Wildt, R. Winter, and F. Zabel, J. Phys. Chem. **87**, 3943 (1983).
[64] D. S. Y. Hsu, W. M. Shaub, T. Creamer, D. Gutman, and M. C. Lin, Ber. Bunsenges. Phys. Chem. **87**, 909 (1983).
[65] J. Berkowitz, G. B. Ellison, and D. Gutman, J. Phys. Chem. **98**, 2744 (1994). We estimate the energy required to abstract a C–H to be about that of ethane, $DH_{298}[CH_3CH_2-H]=101.1\pm0.4$ kcal mol^{-1}. Table V lists the strength of the peroxy OH bond as $DH_{298}[CH_3CH_2OO-H]=85\pm2$ kcal mol^{-1}. Consequently it is endothermic by about 16 kcal mol^{-1} to transfer the H atom from the carbon center to an oxygen center.
[66] W. B. Cook, R. H. Hunt, W. N. Shelton, and F. A. Flaherty, J. Mol. Spectrosc. **171**, 91 (1995).
[67] I. R. Slagle, Q. Feng, and D. Gutman, J. Phys. Chem. **88**, 3648 (1984).
[68] B. S. Jursic, J. Phys. Chem. **101**, 2345 (1997).
[69] K. Saito, R. Ito, T. Kakumoto, and A. Imamura, J. Phys. Chem. **90**, 1422 (1986).
[70] S. P. Walch, Chem. Phys. Lett. **215**, 81 (1993).
[71] G. E. Quelch, M. M. Gallo, and H. F. Schaefer III, J. Am. Chem. Soc. **114**, 8239 (1992).
[72] A. F. Wagner, I. R. Slagle, D. Sarzynski, and D. Gutman, J. Phys. Chem. **94**, 1853 (1990).
[73] G. E. Quelch, M. M. Gallo, M. Shen, Y. Xie, H. F. Schaefer III, and D. Moncrieff, J. Am. Chem. Soc. **116**, 4953 (1994).
[74] I. S. Ignatyev, Y. Xie, W. D. Allen, and H. F. Schaefer III, J. Chem. Phys. **107**, 141 (1997).
[75] S. J. Wyard, R. C. Smith, and F. J. Adrian, J. Chem. Phys. **49**, 2780 (1968).
[76] D. A. Parkes and R. J. Donovan, Chem. Phys. Lett. **36**, 211 (1975).
[77] P. W. Seakins, M. J. Pilling, J. T. Niiranen, D. Gutman, and L. N. Krasnoperov, J. Phys. Chem. **96**, 9847 (1992).

[78] D. Mihelcic, A. Volz-Thomas, H. W. Pätz, D. Kley, and M. Mihelcic, J. Atmos. Chem. **11**, 271 (1990).
[79] L. V. Gurvich, I. V. Veyts, C. B. Alcock, and V. S. Iorish, *Thermodynamic Properties of Individual Substances*, 4th ed. (Hemisphere, New York, 1991).
[80] N. A. Kozlov and I. B. Rabinovich, Trudy Po Khimii I Khimicheskoi Tekhnologii, 189 (1964).
[81] M. W. Chase Jr., C. A. Davies, J. R. Downey Jr., D. J. Frurip, R. A. McDonald, and A. N. Syverud, J. Phys. Chem. Ref. Data 14 (Suppl. No. 1), 1 (1985), JANAF Thermochemical Tables.
[82] L. V. Gurvich, I. V. Veyts, C. B. Alcock, and V. S. Iorish, *Thermodynamic Properties of Individual Substances*, 4th ed. (Hemisphere, New York, 1991).
[83] J. B. Pedley, R. D. Naylor, and S. P. Kirby, *Thermochemistry of Organic Compounds*, 2nd ed. (Chapman and Hall, New York, 1986).
[84] S. W. Benson, *Thermochemical Kinetics*, 2nd ed. (Wiley, New York, 1976).
[85] D. L. Baulch, R. A. Cox, R. F. Hampson Jr., J. A. Kerr, J. Troe, and R. T. Watson, J. Phys. Chem. Ref. Data **13**, 1259 (1984).
[86] The correction from $\Delta_f H_{298}$ to $\Delta_f H_0$ requires a heat capacity computation and we have used an *ab initio* CBS-Q electronic structure calculation for this evaluation.